Journal of Petroleum Science and Engineering 147 (2016) 181–201

Contents lists available at ScienceDirect

Journal of Petroleum Science and Engineering

journal homepage: www.elsevier.com/locate/petrol

Energy efficiency characteristics in steady-state relative permeability diagrams of two-phase flow in porous media

Marios S. Valavanides *, Eraldo Totaj, Minas Tsokopoulos

Department of Civil Engineering, TEI Athens, Ag. Spyridonos, Athens GR-12210, Greece

ARTICLE INFO

Article history:
Received 5 June 2015
Received in revised form
27 April 2016
Accepted 29 April 2016
Available online 6 May 2016

Keywords:
Two-phase flow
Porous media
Steady-state
Relative permeability diagrams
Energy efficiency
Operational efficiency
Optimum operating conditions
SCAL

ABSTRACT

Experimental evidence on the phenomenology of steady-state two-phase flow in porous media processes is recorded in the conventional relative permeability diagrams. In the present work, the hypothesis on the existence of steady-state flow conditions, for which the energy efficiency of two-phase flow in porous media processes attains a maximum value, has been tested against available laboratory data. The energy efficiency of the process is considered with respect to the oil transport over the mechanical power supplied to it or, "oil produced per kW of mechanical power dissipated in pumps", appropriately reduced to a dimensionless variable, namely the energy utilization factor. Relative permeability data sets were acquired from a total of 179 relative permeability diagrams in 35 published laboratory studies, pertaining to a variety of steady-state two-phase flow conditions and types of porous media. The acquired data were then transformed into energy efficiency data sets for the corresponding system and flow settings. The transformation stems from the Darcy fractional flow relations, combined with the equality between the flowrate and mobility ratio observed when steady-state conditions are maintained. The objective of the present work is to reveal and provide extensive experimental evidence on the existence of optimum operating conditions as well as on distinct trends of the energy efficiency over the pertinent flow regimes and system configurations. Areas of critical relevance that have not been investigated or require further investigation are also highlighted.

1. Introduction and scope of work

Two-phase flow in porous media is a physical process whereby two phases simultaneously flow within a porous medium. When the flow is immiscible (i. e. the two phases do not mix), one of the phases is wetting the interstitial surface of the porous medium against the other, non-wetting phase. The wetting phase is conventionally referred to as "water" and the non-wetting phase as "oil". The combined effect of wetting and interfacial tension is the disconnection of the non-wetting phase into fluidic elements of smaller or larger size – compared to the average pore size. Two-phase flow in porous media occupies a central position in physically important processes with practical applications of industrial and environmental interest, such as: enhanced oil recovery (Lake, 1989; Alvarado and Manrique, 2010), carbon dioxide sequestration (Burnside and Naylor, 2014), groundwater and soil contamination and subsurface remediation (Khan et al., 2004), the operation of multiphase trickle-bed reactors (Van de Merwe and Nicol, 2009), the operation of proton exchange membrane fuel cells (Bazylak, 2009), etc. The majority of those applications are based on inherently transient processes whereby one phase displaces the other. Drainage is said to occur when a non-wetting phase (oil) enters the pore network to displace a wetting phase (water), whereas imbibition occurs if the latter displaces the former. Drainage and imbibition are predominantly *transient* processes: the pattern structure of the two fluids, as to their distribution within the network and to the disconnectedness of the non-wetting phase (oil), change during the process. In addition, averages of physical quantities -taken over any volume larger than the representative elementary volume (REV)- change with position and time. For example, the average saturation of the wetting phase over any region of the pore network increases with time as a wetting fluid (water) is replacing a non-wetting fluid (oil) during the imbibition process.

To understand the physics of such processes in a deeper context, we need first to understand the *steady-state flow*, whereby the two immiscible fluids, oil (the non-wetting) and water (the wetting), are forced to flow at pre-selected, constant flowrates. In this second class of processes, physical quantities also change with time, but in a different way: averages remain practically constant or their variability is extremely small, i. e. the variation of the local

* Corresponding author.
E-mail address: marval@teiath.gr (M.S. Valavanides).
URL: http://users.teiath.gr/marval/index_en.html (M.S. Valavanides).

http://dx.doi.org/10.1016/j.petrol.2016.04.039
0920-4105/

Nomenclature

Symbols, indices

$\sim$	A tilde indicates a dimensional variable (no tilde denotes a dimensionless variable)
Δ^*	small difference of variable *
$\{^*\}$	set of * values
o	"oil" or non-wetting phase (index)
w	"water" or wetting phase (index)

Physical variables – Latin letters

Ca	Capillary number
$\tilde{e}$	energy efficiency of the process
f	fractional flow
f_{EU}	energy utilization factor
$\tilde{k}$	absolute permeability of the porous medium
$\tilde{p}$	macroscopic pressure
r	oil/water flowrate ratio
S_w	wetting phase saturation
$\tilde{q}$	flowrate
$\tilde{U}$	superficial velocity
W	reduced rate of mechanical energy dissipation
x	reduced macroscopic pressure gradient
$x_{\text{p.m.}}$	vector containing the geometrical and topological parameters of the pore network
$\tilde{z}$	position length along the macroscopic flow direction

Physical variables - Greek letters

$\tilde{\gamma}_{ow}$	oil-water interfacial tension
κ	oil/water viscosity ratio
$\tilde{\lambda}$	mobility
$\tilde{\mu}$	dynamic viscosity

value (in time and space) is very small compared to the average value. The flow structure -comprising a mixture of connected and disconnected fluidic elements moving at different velocities- incessantly rearranges itself within a phase space of physically admissible flow configurations (Avraam and Payatakes, 1995; Erpelding et al., 2013). According to ergodicity principles, the time average of the flow is the same as its phase space average over all physically admissible configurations (Valavanides, 2012).

Two-phase flow in porous media is ubiquitous in industrial applications. Particular attention is given on tuning the design parameters and process interventions so as to increase the "sweeping efficiency", i. e. the extraction of one phase (residing in-situ) and its replacement by another phase - wetting or non-wetting depends on the particular application. In this context, the decrease of saturation has become the main objective in process optimization (whether recovery, substitution, removal etc.). Nevertheless, at present, pragmatic sustainability issues on energy production/management (hydrocarbons, fuel cells, catalytic or trickle-bed reactors) shifts "recovery optimization" trends into "energy /cost efficiency optimization" scopes and targets (Charpentier, 2007; Clayton, 2014). As a consequence, new challenges emerge within a wide spectrum of technological problems, extending from laboratory to industrial scale, e. g. unconventional/enhanced oil recovery /carbon capture and sequestration processes, soil and aquifer pollution and remediation, operation of trickle-bed reactors [Valavanides et al., 2015a, 2015b]. To address these issues we need first to examine if any *energy efficiency* characteristics are inherent in the sought process, starting from its simpler form, immiscible steady-state.

The scope of the present work is to collect data from published laboratory studies of steady-state two-phase flow in porous media, in order to examine if there exists any operational characteristics related to the energy efficiency of the process, if such characteristics show a universal trend and if that trend can be exploited in a systematic way. The objective and driving force for this work, was to provide extensive experimental evidence on the predictions of the mechanistic model *DeProF*, that first revealed the existence of optimum operating conditions as well as other latent operational characteristics of two-phase flow in porous media.

The *DeProF* model has been developed by Valavanides & Payatakes (ca 1998). The purpose was to develop a mechanistic model that could explain (on physical principles) the various interstitial flow arrangements observed in the laboratory study of Avraam and Payatakes (1995). It turned out that the model was self-contained and rigorous enough to be further exploited as a simulating tool having the capability of revealing latent process characteristics. Such a characteristic is the existence of the locus of maximum operational efficiency of the process (Valavanides and Payatakes, 2003). To verify the validity of the *DeProF* model predictions, a preliminary laboratory proof was presented in a review of the progress in the development of the *DeProF* tentative theory (Valavanides, 2012). The paper presented past efforts and new results, highlighted critical issues and suggested future steps to be taken. With respect to laboratory verification of the *DeProF* model predictions, it referenced the examination of 23 relative permeability diagrams in total, from 7 published laboratory studies. That examination was preliminary and only indicative of the latent information one could extract from such diagrams.

It is well understood that two-phase flow in porous media is a complicated multi-parametric process extending across different scales and comprising a hierarchical system (Cushman, 1997; Payatakes et al., 1998; Perez-Mercader, 2004). Therefore, any attempt to describe it by developing a rigorous analytical model (overtaking any phenomenological description) requires, *a-priori*, the collection of an adequate number of laboratory data. Then, areas over the parameter domain being void of laboratory data should be filled and missing data should be recovered by designing more efficient laboratory studies. Such tasking should deploy in parallel to the development of "better" models.

As already stated, the scope of the present work is to provide extensive experimental evidence and reveal critical process characteristics with respect to energy efficiency.

On this purpose, the present work examines 35 laboratory studies and 179 diagrams, stretching across a broad range of types of porous media, fluids and flow conditions. The existence of optimum operating conditions taken apart, there are additional characteristics that need to be revealed, explained on physical considerations and then rationally justified on the provision of rigorous theoretical background. Said particular characteristics have been only recently identified and will be presented in the following sections. The extent, diversity and volume of collected laboratory data is the seed material for creating a tentative database that will provide the necessary laboratory strings of evidence (or, the vital clues) for revealing latent universal characteristics of the sought process.

In the following, we will present the concept of operational efficiency of steady-state two-phase flow in porous media and the corresponding predictions provided by the *DeProF* model

(Section 2). Next, in the main part of the work, we will present the experimental evidence substantiating the *DeProF* model predictions (Section 3) and give an outline of the basic results (Section 4). Finally, we will conclude with suggestions for future work.

2. Modeling and analytical considerations

2.1. Relative permeability

The concept of relative permeability is basic when two immiscible phases flow simultaneously within a porous medium. It has been contrived to extend Darcy's law in accounting the phenomenology of the process. The so-called fractional form of Darcy's law provides the phenomenological (cause-effect) relation describing the process. It is written as

$$\tilde{U}_i = k_{ri}\frac{\tilde{k}}{\tilde{\mu}_i}\left(-\frac{\Delta\tilde{p}}{\Delta\tilde{z}}\right)_i \qquad i = o, w \tag{1}$$

where.

$\tilde{U}_o$ and $\tilde{U}_w$ are the superficial velocities of "oil" (the non-wetting phase) and "water" (the wetting phase), e. g. oil/water, gas/oil, etc,.

$\tilde{k}$ is the absolute permeability of the porous medium,.

$\tilde{\mu}_o$, $\tilde{\mu}_w$ are the dynamic viscosities of the two phases and.

$(-\Delta\tilde{p}/\Delta\tilde{z})_i$ denotes the macroscopic pressure gradient in each phase-i.

k_{ro} and k_{rw} denote the relative permeability of oil and water respectively. They are both dimensionless variables, taking values between 0 and 1. The relative permeability of each phase i, provides a measure of the reduction in the specific permeability of phase-i due to the *presence* and *mobility* of the other phase-j in the porous medium.

In general, relative permeabilities are measured either by *steady-state* or *unsteady-state* methods (for a brief review of the methods commonly used to determine relative permeability, see Honarpour et al., 1986, also Müller , 2011). In steady-state methods, the two-phases are simultaneously injected at a fixed ratio into a porous medium. When the system reaches steady-state conditions (i. e. when averages do not change with time), the differential pressures are measured and the relative permeabilities can be calculated by using Darcy's law, Eq. (1). Steady-state methods are in general relatively accurate, easy to understand and implement straightforward and acceptable data processing procedures, namely regular/special core analysis [API, 1998]. However, since the process needs to reach steady-state conditions, steady-state methods, in general, are time-consuming. Relative permeability diagrams are produced for a given porous medium and for a given pair of fluids by laboratory measurements when different flow conditions are imposed. Conventionally, relative permeability values are plotted in terms of the corresponding measured values of the wetting phase saturation, S_w, to derive the well-known relative permeability diagrams. The latter provide the necessary data input in reservoir studies when estimating the producible reserves and design flooding/sweeping interventions for ultimate recovery. The use of saturation, S_w, as the independent variable is entirely conventional. The issue will be discussed in the following sections.

2.2. Energy efficiency aspects of two-phase flow in porous media

Consider the simultaneous flow of oil and water through a pore network. The oil-water flowrate ratio, r, is defined as

$$r = \frac{\tilde{q}_o}{\tilde{q}_w} = \frac{\tilde{U}_o}{\tilde{U}_w} \tag{2}$$

In order to induce and sustain specific flowrates of oil, $\tilde{q}_o$, and water, $\tilde{q}_w$, corresponding pressure differences, $\Delta\tilde{p}_o$ and $\Delta\tilde{p}_w$, must be continuously effected upon the two phases. Consequently, an amount of mechanical power, $\tilde{W}$, equal to

$$\tilde{W} = \tilde{q}_o\Delta\tilde{p}_o + \tilde{q}_w\Delta\tilde{p}_w \tag{3}$$

must be externally supplied to the system, to balance the rate of mechanical energy dissipation within the process. The later is caused interstitially by the bulk viscous stresses in combination with the local rates of deformation, and, by the velocities of oil/water menisci moving against local capillary pressure differences induced by contact angle hysteresis effects. For a fixed oil/water/p. m. system, and for externally imposed flowrates, the magnitude of the two contributions depends primarily on the saturation (bulk volume fractions) and on the degree of disconnection of the non-wetting phase (specific surface of o/w interface). The former regulates the pressure drop attributed to viscosity. The latter regulates the induced pressure drop that is attributed to the motion of interfaces – due to the hysteresis between receding and advancing contact angles, as each disconnected oil blob flows through the network of conducting pores. On the macroscopic scale, the net pressure drop across receding and advancing interfaces is added to the viscosity induced pressure drop within all the disconnected fluidic elements. In general, i. e. for any oil/water/p.m. system, the relative contribution of the aforementioned effects depends on the structure of the pore network in combination to the physicochemical characteristics pertaining to the interaction between the two fluids and the solid matrix (viscosity ratio, interfacial tension, contact angles hysteresis etc.).

The capillary number, *Ca*, defined as

$$Ca = \tilde{\mu}_w\tilde{U}_w/\tilde{\gamma}_{ow} \tag{4}$$

where $\tilde{\gamma}_{ow}$ the interfacial tension between the two phases, provides a relative measure of the viscous forces over the capillary forces.

Ca and *r*, are considered as the *operational* or *flow parameters* of the process. The set of process parameters is complemented by the set of *system parameters*, namely, the absolute permeability and other geometrical, topological and structural –bulk or surface-characteristics of the pore network, the bulk viscosities, the interfacial tension as well as the physicochemical characteristics of the two phases (contact angles, wetting, chemical potential etc.). As their name suggests, the operational parameters can be regulated during the process whereas –in general- system parameters cannot. The flow parameters can be considered as the independent variables in the phenomenological (cause-effect) relation (1) that describe the process. In that case, system parameters are considered to be fixed.

Now, consider a reference one-phase flow of water, at a flowrate equal to

$$\tilde{q}^{1\Phi} = \tilde{q}^{w} \tag{5}$$

Considering the superficial velocity of water and the corresponding capillary number value, we may define a characteristic rate of mechanical energy dissipation for this reference one-phase flow as

$$\tilde{W}^{1\Phi} = \frac{(\tilde{\gamma}_{ow}Ca)^2}{\tilde{k}\tilde{\mu}_w} \tag{6}$$

Therefore, we can define the reduced rate of mechanical energy dissipation within the process, W, as

$$W = \frac{\tilde{W}}{\tilde{W}^{1\Phi}} = \tilde{W}\frac{\tilde{k}\tilde{\mu}_w}{(\tilde{\gamma}_{ow}Ca)^2} \tag{7}$$

The efficiency of the process is defined as the ratio of the recovered-oil flowrate, $\tilde{q}_o = \tilde{U}_o\tilde{A}$, over the mechanical power dissipation, $\tilde{W}$. Both quantities are considered within a porous medium control volume, $\Delta\tilde{V} = \tilde{A}\Delta\tilde{z}$. Therefore the specific (volumetric or per unit volume of porous medium) efficiency can be expressed as $\tilde{e} = \tilde{U}_o\tilde{A}(\tilde{W}\tilde{A}\Delta\tilde{z})^{-1}$. A dimensionless macroscopic variable, can be defined by reducing $\tilde{e}$ with the respective volumetric efficiency for one-phase flow conditions, $\tilde{e}^{1\Phi} = \tilde{U}_w\tilde{A}(\tilde{W}^{1\Phi}\tilde{A}\Delta\tilde{z})^{-1}$. This dimensionless macroscopic variable, namely the energy utilization factor, f_{EU}, is readily expressed as

$$f_{EU} = \frac{\tilde{e}}{\tilde{e}^{1\Phi}} = \frac{\tilde{U}_o\tilde{W}^{1\Phi}}{\tilde{U}_w\tilde{W}} = \frac{r}{W(Ca, r)} \tag{8}$$

Expression (9) is a reduced measure of the efficiency of the process, with respect to the oil transport over the mechanical power supplied to it or "oil produced per kW of mechanical power dissipated in pumps". It was originally defined by Valavanides and Payatakes (2003) in the context of the development of the *DeProF* mechanistic model (see Appendix A).

2.3. Independent variable of the process: saturation or flow conditions?

Since we have considered the simultaneous flow of both phases at predetermined flowrates and, so long as the values of the system parameters are fixed, then, a two-dimensional set, comprising either $\{U_o, U_w\}$, or $\{Ca, r\}$ must be used as the set of independent variables. In the same context, a set of independent variables may be defined by the (two) capillary numbers $\{Ca_o, Ca_w\}$ pertaining to the superficial velocity of oil and water (Tsakiroglou et al., 2015). It is clear that the transition between the two sets is provided as $\{Ca, r\}\equiv\{Ca_w, Ca_o/Ca_w\}$.

In the reservoir engineering domain there is still reluctance in using the flow conditions as the independent variable(s). The applicable standard is to refer to one of the fractional flows, of oil, f_o, or water, f_w. The latter are complementary defined as

$$f_o = \frac{\tilde{q}_o}{\tilde{q}_o + \tilde{q}_w} = \frac{r}{1+r} \quad \text{and} \quad f_w = \frac{\tilde{q}_w}{\tilde{q}_o + \tilde{q}_w} = \frac{1}{1+r} \tag{9}$$

In the present work, the use of the flowrate ratio, r, instead of the fractional flow as independent variable, was decided because it has the advantage of a more convenient description of the sought physical process. We will refer to this issue later on, in paragraph 3.2.3.

Before proceeding to the next section, a remark must be made with reference to the conventional use of saturation as the independent variable of the process. It is based on the perception that disconnected oil blobs and other fluidic elements (ganglia and/or droplets) do not move with the average flow but remain stranded in the pore medium matrix. This situation arises when flow conditions of relatively "small values" of the capillary number are maintained. Only in those cases would the disconnected oil block or plug part of the available flow cross-section, by a fraction analogous to the average saturation. Nevertheless, there is ample experimental evidence that disconnected flow is a substantial and sometimes prevailing flow pattern (Tsakiroglou et al., 2007; Tallakstad et al., 2009; Georgiadis et al., 2013, Youssef et al., 2014). Now, a particular value in saturation does not necessarily imply that a unique disconnected structure (arrangement) of the non-wetting phase will settle in. Disconnected structures of the non-wetting phase can be coarsely described by a spectrum of population densities comprising "many-and-small" or "fewer-and-larger" fluidic elements (ganglia and droplets). For any one of those cases, the corresponding superficial velocity of the non-wetting phase would not necessarily attain the same value. The latter would be the result of the dialect over the mass and momentum balances between the two factors inhibiting the transport of each phase, viscosity and capillarity, within the particular porous medium structure and for the externally imposed flow conditions. As a consequence, the corresponding effective permeabilities would differ and, therefore, the corresponding values of the relative permeability to the non-wetting phase would be different. Those different values of the relative permeability would correspond to the same saturation value. Therefore, treating relative permeabilities as a function of the saturation can only be considered as a misconceived grasping of the whole picture. After all, saturation is measured, not externally imposed. If one wants to describe the process in the entire flow regime (extending across extreme values in the capillary number and the viscosity ratio), it has to consider those variables that describe the externally imposed conditions and contain macroscopic kinematic information (e. g. the superficial velocity of each phase or, equivalently, the capillary number and the flow rate ratio). In addition, saturation represents macroscopic static information and cannot adequately (or uniquely) describe the flow conditions. It brings no definite input to the momentum balance.

2.4. The DeProF mechanistic model for steady-state two-phase flow in pore networks

The mechanistic model *DeProF* for immiscible steady-state two-phase flow in pore networks (Valavanides, 2012), can be used to predict the relative permeability of each phase. It is based on the concept of decomposition in prototype flows. The model takes into account the pore-scale mechanisms and the sources of non-linearity caused by the motion of interfaces, as well as other complex, network-wide cooperative effects, to estimate the conductivity of each class of pore unit cells. It implements effective medium theory with appropriate expressions for pore-to-macro scale consistency for oil and water mass transport, to derive an implicit algebraic relation invoking the macroscopic pressure gradient, the capillary number and the flow-rate ratio, in terms of the pertinent system parameter (physichochemical, topological) describing the oil-water-porous medium system.

Using the *DeProF* model, and implementing any ordinary numerical equation solver, one can obtain the solution to the problem of steady-state two-phase flow in porous media in terms of the capillary number, Ca, the oil/water flowrate ratio, r, the oil/water viscosity ratio, κ, here defined as,

$$\kappa = \tilde{\mu}_o/\tilde{\mu}_w \tag{10}$$

the advancing and receding contact angles, and a parameter vector, comprising not only the absolute permeability, but also dimensionless parameters that describe the geometrical and topological characteristics of the porous medium affecting the flow.

Extensive simulations using the *DeProF* model algorithm, revealed that a continuous line, $r^*(Ca)$, exists in the (Ca, r) domain for which the energy utilization index, Eq. (8), takes locally maximum values (Valavanides and Payatakes, 2003). This line appears when the ridge of the $f_{EU}(Ca,r)$ surface is projected on the (Ca, r) plane, see Fig. 1, whereby the effect of Ca and r on the energy utilization index, f_{EU}, is depicted by mountain-range shaped surfaces). It appears that for every system of fluids (different values of the viscosity ratio, κ), there exists a continuous line in the (Ca, r) domain for which the energy utilization factor takes locally maximum values. This line is the projection of the r/W surface ridge on the (Ca, r) plane. For every constant value of Ca, there exists a particular value of the flowrate ratio, $r^*(Ca)$, for which the energy utilization factor becomes maximum. In other words, oil flowrate per kW of power externally

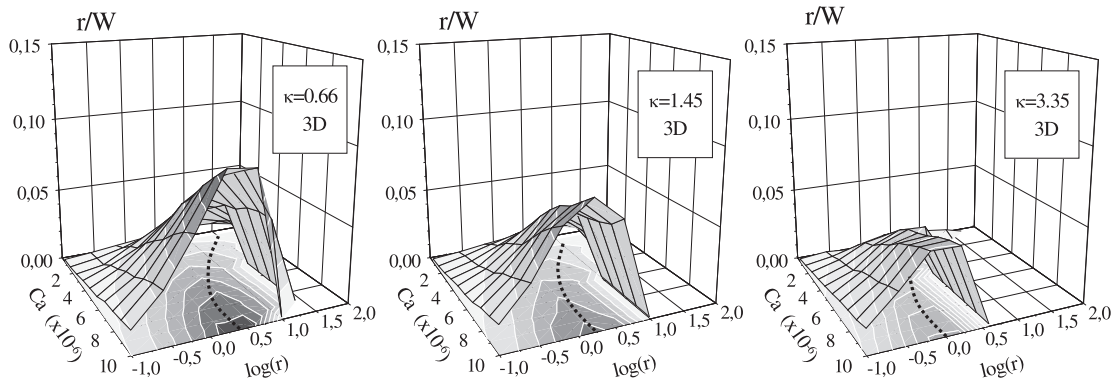

Fig. 1. Energy utilization factor, $f_{EU}=r/W$, as a function of Ca and r. The diagrams pertain to 3D pore network *DeProF* simulations for two o/w systems with viscosity ratios $\kappa=0{,}66$, 1,45 and 3,35 (Valavanides, 2012). The dashed lines represent the projection of the ridge of the $f_{EU}(Ca, r)$ surface on the (Ca, r) plane. These lines define the loci $r^*(Ca)$ of the optimum operating conditions for the three systems considered.

supplied to the system attains maximum values.

The existence of 'optimum conditions' for oil transport in two-phase flow in pore networks is a consequence of the remarkable internal adaptability of the flow to externally imposed flow constraints (Ca, r) and its inherent characteristic in self adjusting the connected versus disconnected moving-oil balance (mass- and momentum- wise). Detecting and setting such conditions is of ample importance in real processes of industrial scale. It is therefore imperative to challenge the *DeProF* theory claims regarding the existence of optimum operating conditions (OOC) in such processes. In the present work we will provide the necessary experimental evidence by tapping the data contained within a variety of published laboratory studies pertaining to steady-state two-phase flows in porous media. To do so, we need first to transform relative permeability values into energy utilization data.

2.5. Transformation of relative permeability (k_{ro}, k_{rw}) into operational efficiency (f_{EU})

The transformation,

$$r = \frac{\tilde{q}_o}{\tilde{q}_w} = \frac{\tilde{U}_o}{\tilde{U}_w} = \frac{k_{ro}/\tilde{\mu}_o}{k_{rw}/\tilde{\mu}_w} = \frac{\tilde{\lambda}_o}{\tilde{\lambda}_w} = \frac{1}{\kappa}\frac{k_{ro}}{k_{rw}} \tag{11}$$

$$f_{EU} = \frac{k_{ro}}{\kappa(r+1)} = \frac{rk_{rw}}{r+1} = f_o k_{rw} = k_{ro}\left(\frac{k_{ro}}{k_{rw}} + \kappa\right)^{-1} \tag{12}$$

originally introduced by Valavanides (2012), is valid for steady-state two-phase flows in porous media. In Eq. (11), $\tilde{\lambda}_o$, $\tilde{\lambda}_w$, denote the mobility of oil and water, defined as

$$\tilde{\lambda}_o = k_{ro}/\tilde{\mu}_o \quad \text{and} \quad \tilde{\lambda}_w = k_{rw}/\tilde{\mu}_w \tag{13}$$

For the sake of self-sufficiency of the present work, a derivation of Eqs. (11, 12) is presented in the Appendix. The proof is based on the observation that in steady-state conditions, the pressure gradient is the same in both phases, or, equivalently, the mobility ratio equals the flowrate ratio (Valavanides, 1998; Avraam and Payatakes, 1999). By plotting flowrate ratio values against the mobility ratio values pertaining to steady-state conditions, the corresponding data points align along the diagonal. This statement can be used to test/validate the consistency of steady-state relative permeability diagrams as long as the flowrate ratio values are disclosed or can be estimated. If a data point is not aligned with the rest of the group this would not correspond to steady-state conditions. In general, data alignment can be evaluated by implementing appropriate least-squares fitting techniques.

Here, the transformation given by Eqs. (11, 12) was implemented to reconstruct measured relative permeability vs saturation data sets, $\{k_{ro}, k_{rw}, S_w\}$, into corresponding data sets of energy utilization vs flowrate ratio, $\{f_{EU}, r\}$.

A typical reconstruction of $\{k_{ro}, k_{rw}, S_w\}$, into $\{f_{EU}, r\}$ data sets is presented in Fig. 2, whereby steady-state relative permeability diagrams published in Bentsen, 2005, are transformed into energy utilization diagrams. Details on the procedure of the transformation are described in the following section.

A handy spreadsheet that automatically transforms conventional steady-state relative permeability diagrams into energy efficiency diagrams, $f_{EU}(r)$, can be downloaded from the internet (Valavanides, 2013). This spreadsheet transformer also contains a diagram where measured flowrate ratio values, $r = \tilde{q}_o/\tilde{q}_w$ are plotted against computed values, $r = \tilde{\lambda}_o/\tilde{\lambda}_w = k_{ro}/\kappa k_{rw}$, to visualize or confirm whether steady-state flow conditions had settle during data collection in the particular laboratory run.

3. Materials and methods

3.1. Laboratory studies of steady-state two-phase flow in porous media

Laboratory studies of two-phase flow in pore networks have been traced in databases (SCOPUS, OnePetro/SPE) and other professional society resources (SPE, SPWLA, SCA, etc.) or laboratory webpages. The search revealed 35 published laboratory studies comprising a total of 179 laboratory runs, pertaining to steady-state flows of different pairs of wetting and non-wetting fluids in sand packs, plug cores, glass micromodels and virtual pore-network models, including computational fluid dynamics (CFD) or lattice Boltzmann (LB) simulations (virtual pore network flows). The number of studies implementing unsteady-state conditions is larger –due to the comparatively easier methodology- and will eventually be the subject of a future work.

A brief description of the selected studies is presented in the following. A coarse classification of the pertinent relative permeability diagrams is presented in Table 1, whereas a tabulated listing of materials and methods is outlined in Table 2.

- Allen and Pucket, 1986, have compared laboratory measurements of steady state and dynamic brine/tetradecane immiscible displacements with significant capillarity effects in sandstone cores, to theoretical predictions implementing Eulerian and Lagrangian methods.
- Avraam and Payatakes, 1995 and 1999, in their systematic study of steady-state two-phase flow in glass pore networks revealed

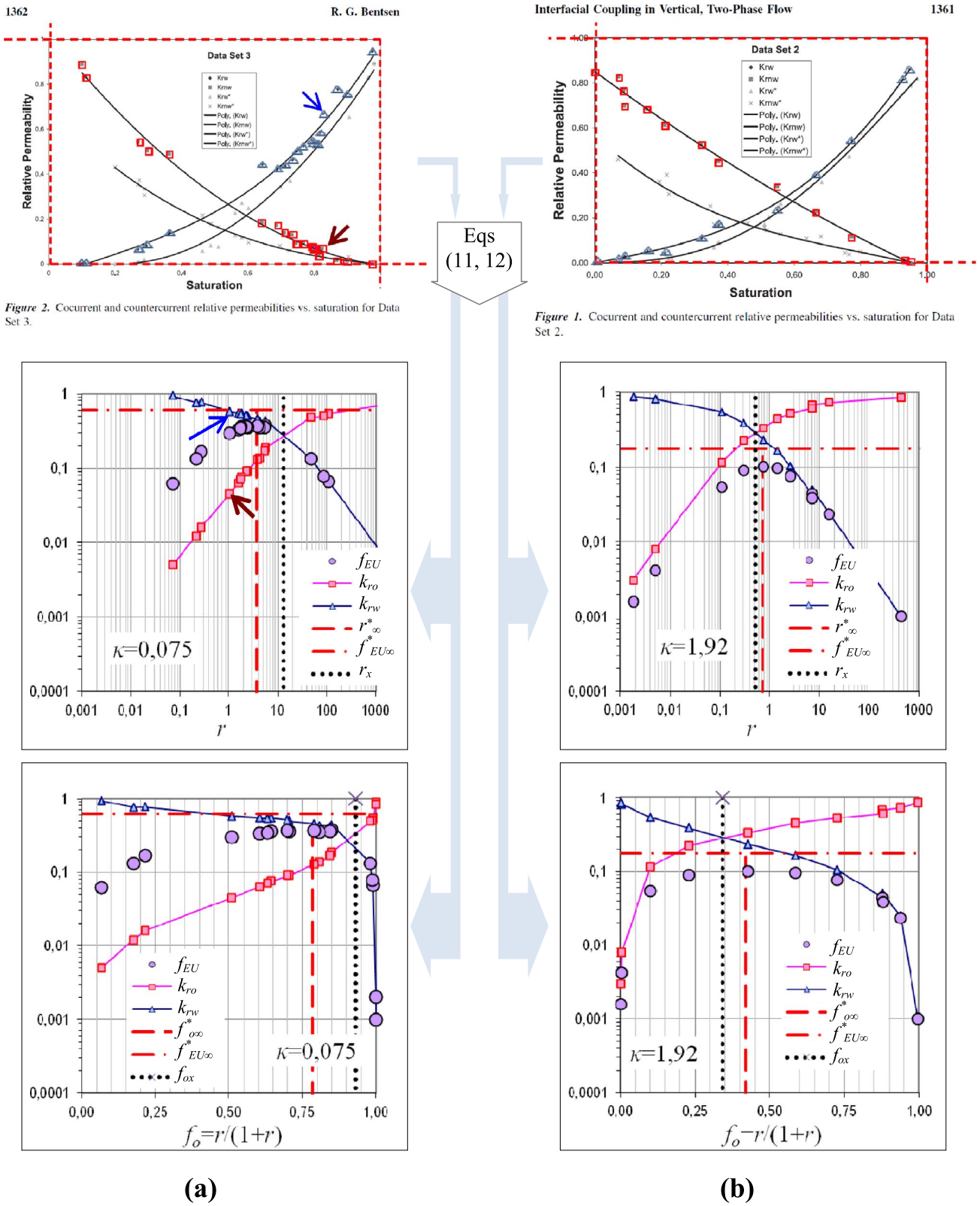

Fig. 2. Typical transformations of relative permeability data diagrams for oil, k_{ro} (□), and water, k_{rw} (△) into energy utilization index, f_{EU}, (○) against the flowrate ratio, r, (and the oil fractional flow, f_o) data diagrams. The relative permeability data values pertain to two typical systems: (a) favorable viscosity ratio and (b) unfavorable viscosity ratio. (Source relative permeability diagrams, Bentsen, 2005.)

the flow regimes settling in mixed connected and disconnected oil flow.

- Beckner et al., 1988, have tried to simulate numericaly the flow behavior in fractured oil reservoir cores using as a benchmark data from a laboratory experiment involving a matrix-fracture system.
- Bennion and Bachu, 2005, presented detailed water - super-critical CO_2 relative permeability data for various cores from

Table 1
Examined relative permeability diagrams pertaining to a variety of steady-state flows in sand packs, plug cores, glass micromodels and virtual p.m. and fluid systems.

Core plug type	Lab runs	Viscosity ratio, $\kappa = \tilde{\mu}_o/\tilde{\mu}_w$	Lab runs
Berea sandstone	48	Favorable, $\kappa < 1$	67
Nellie Bly sandstone	4	$\kappa = 1$	15
Bentheimer sandstone	13	Unfavorable, $1 < \kappa$	97
Clashach sandstone	1	**In total**	**179**
Other consolidated sandstone	8		
Loudon core	3		
Consolidated rock core samples	16		
Teflon (consolidated, porous)	3		
Propant pack	2		
Carbonate core	31	**Constant Ca runs**	**73**
Sandpacks (incl. crushed Pyrex™)	10		
Glass pore network models	15		
Outcrop chalk	2		
Real pore networks subtotal	**156**		
Virtual runs (LB or CFD simulations)	23		
In total	**179**		

sandstone and carbonate formations in potential sequestration zones in the Western Canada sedimentary basin.

- Bentsen, 2005, used the laboratory data from two sets of gravity-driven, steady-state, co-current and countercurrent flow experiments in crushed Pyrex packs to test the interfacial coupling theory for immiscible steady-state two-phase flow and to analyze the effects of interfacial and viscous coupling.
- Braun and Blackwell, 1981, performed relative permeability measurements on preserved core samples at reservoir temperature and pressure, using reservoir fluids at different flow rate ratios.
- Dernaika et al., 2012, recently presented the results of a systematic laboratory study pertaining to the measurement of primary drainage and imbibition water-oil relative permeability (bounding) curves, using live fluids, at full reservoir conditions. They have used cores and plugs of five rock types, obtained from a cretaceous carbonate reservoir. This is the most extensive examination of carbonate cores in one publication.
- Eleri et al., 1995, performed steady- as well as unsteady-state relative permeability experiments on restored-state carbonate reservoir cores to study the impact of different test methodologies on relative permeability curves, hysteresis and residual oil saturations.
- Fulcher et al., 1985, studied the effect of the capillary number on two-phase flow in fired Berea sandstone core plugs.
- Geffen et al., 1951, performed laboratory experiments to establish the effects of pressure gradient and saturation history on the measurement of oil/brine relative permeability in sandstones.
- Ghassemi and Pak, 2011, implemented the lattice Boltzmann method to study the factors influencing the relative permeabilities of two immiscible fluids with favorable, unfavorable and equal viscosity ratios.
- Kleppe and Morse, 1974, developed a numerical model to study the flow behavior of fractured oil reservoirs produced by water displacement, which was then benchmarked against data from a laboratory experiment involving a matrix-fracture system.
- Lai and Miskimins, 2010, measured gas-water relative permeabilities for propant packs under high confining stress conditions.
- Leverett, 1939, in one of the earliest systematic laboratory studies, examined the effect of viscosity, interfacial tension and sand packing on the flow of oil-water mixtures through unconsolidated sands.
- Li et al., 2005, used a 3D parallel processing version of a two-fluid-phase lattice-Boltzmann (LB) model to investigate the importance of viscous coupling effects, caused by momentum transfer between the two immiscible fluid phases in porous systems.
- Lo and Mungan, 1973, studied the effect of temperature on water-oil relative permeabilities in oil-wet and water-wet systems.
- Maloney et al., 1993, report the results from special core analyses (SCAL) and gas/water and oil/water relative permeability measurements conducted on samples of rock.
- Masalmeh, 2003, studied the effect of wettability heterogeneity on capillary pressure and relative permeability.
- Nordtvedt et al., 1994, developed and tested a method for the simultaneous determination of relative permeability and capillary pressure from transient and equilibrium data gathered during steady state experiments. Two sets of production and pressure drop data -one simulated and one experimental- have been analyzed.
- Oak et al., 1990, measured two and three-phase relative permeabilities on a water-wet fired Berea sandstone core.
- Odeh, A.S., 1959, provided a theoretical analysis to determine the effect of viscosity ratio between the non-wetting and the wetting phase on relative permeability. He conducted a laboratory study in four natural cores from consolidated rock with various oils of different viscosity, to test the validity of the derived equations.
- Perrin et al., 2009, measured steady-state relative permeabilities in two different rock samples and CO_2/brine systems over a range of injection flow rates. They studied the effect of core heterogeneity and flowrate on the efficiency of multi-phase brine displacement, on the CO_2 saturation and on the relative permeabilities.
- Ramstad et al., 2012, studied the relative permeability functions derived from two-phase lattice Boltzmann (LB) simulations on X-ray microtomography pore space images of Bentheimer and Berea sandstones and benchmarked it with available steady-state, drainage and imbibition flow experimental data.
- Reynolds et al., 2014, recently presented the results of a systematic laboratory study of drainage core floods using CO_2/brine and N_2/water on a single heterogeneous Bentheimer sandstone rock core.
- Richardson et al., 1952, performed a comparative study of a number of methods of relative permeability measurement, in a search for the technique most suited to routine analysis of cores taken from reservoir rock.
- Sandberg et al., 1958, studied the effect of fluid flow rate and fluid viscosity on oil-water relative permeability in homogeneous small core samples taken from sandstone outcrop formations.
- Shafer et al., 1990, combined steady-state and unsteady-state measurements on carbonates, siltstone and sandstone plugs and composite cores.
- Sheng et al., 2011, provided numerical predictions of relative permeability from microCT images implementing pore network simulation with different algorithms – quasi-static /steady-state /unsteady-state.
- Talash, 1976, provided an experimental study of the effect of miscibility conditions, implementing the displacement and the steady-state methods in fired Berea cores for a crude oil-water system containing tension reducing additives (surfactants).
- Tsakiroglou et al., 2015, measured relative permeabilities of equal viscosity fluids co-injected in sand-packs to establish the dependence of the relative permeability of oil and water on

Table 2
Detailed listing of materials and methods implemented in the re-examined laboratory studies pertaining to a variety of steady-state flows in sand packs, plug cores, glass micromodels and virtual p.m. and fluid systems.

	Lab study	Source Ref.	pore network type	Φ	$\tilde{k}$ (md)	Fluids	$\tilde{\gamma}_{ow}$ (d/cm)	κ	Comments
				porosity	Absolute permeability	non-wetting / wetting	Interfacial tension	Viscosity ratio	
1	Allen & Pucket, 1986	(run8)	Clashach sandstone	0,21	1520	oil / water(brine10%)	n/a	1,882	Const. flowrate
2	Avraam & Payatakes, 1995	Table 2 & Fig. 9 a,c,e	glass pore network	0,25	9020	n-12cane / DI water+30% glycerol	22,0	0,657	Constant Ca
						n-12cane / DI water	25,0	1,447	
						n-126ane / DI water	25,0	3,351	
3	Avraam & Payatakes, 1999	Table 3 & Fig.3	glass pore network	0,25	9020	n-12cane / DI water+34% extran	9,5	1,563	Constant Ca
						n-Nonanol / Formamide	4,3	2,878	
4	Beckner et al., 1988	Tables 3, 4	fractured Berea sandstone	0,30	20,0	oil / water	n/a	1,250	simulation
		Tables 1, 2	Berea sandstone	0,23	290,0	oil / brine	n/a	2,300	
5	Bennion & Bachu, 2005	Table 3	Cambrian /Sandstone	0,117	0,55	water-saturated CO_2 / brine	n/a	0,085	detailed water-CO2 rel-perm data for 3 sandstone & 3 carbonate formations
			Cooking Lake /Carbonate	0,099	645		n/a	0,065	
			Nisku /Carbonate	0,097	84		n/a	0,085	
			Wabamun Low k /Carbnt	0,079	0,21		n/a	0,065	
			Ellerslie /Sandstone	0,126	2,2		n/a	0,069	
			Viking /Sandstone	0,125	5,78		n/a	0,072	
		Table 4	High k /Carbonate	0,148	174		n/a	0,065	
			High k, Low T /Carbonate	0,148	174		n/a	0,013	
			High k-Freshw /Carbonate	0,148	174		n/a	0,088	
6	Bentsen, 2005	Fig. 1	Pyrex	0,43	230k	oil+w/spirit/ ZnCl2	1,0	1,917	
		Fig. 2		0,43	230k	perchloroethylene+w/spirit / $ZnCl_2$	15,0	0,075	
7	Braun & Blackwell, 1981	Fig. 5	Berea sandst	0,20	262	oil / water(brine)	n/a	6,786	Const flowrate
8	Dernaika et al., 2012	Figs. 5(a), (b)	Carbonate Rock type RRT1 (#113-#114)	0,17	46,0	live oil / water	n/a	1,30	Const. Ca - drainage
				0,20	21,0				Const. Ca - imbibition
				0,17	46,0				
				0,20	21,0				
			Carbonate Rock type RRT2 (#9-#15)	0,28	11,0	live oil / water	n/a	1,30	Const. Ca - drainage
				0,24	1,75				Const. Ca - imbibition
				0,28	11,0				
				0,24	1,75				
			Carbonate Rock type RRT3 (#22-#72)	0,21	2,08	live oil / water	n/a	1,30	Const. Ca - drainage
				0,21	2,06				Const. Ca - imbibition
				0,21	2,08				
				0,21	2,06				
			Carbonate Rock type RRT4 (#4-#6)	0,23	5,34	live oil / water	n/a	1,30	Const. Ca - drainage
				0,21	3,02				Const. Ca - imbibition
				0,22	5,34				
				0,21	3,02				
			Carbonate Rock type RRT5 (#138-#139)	0,18	0,98	live oil / water	n/a	1,30	Const. Ca - drainage
				0,18	1,01				Const. Ca - imbibition
				0,18	0,98				
				0,18	1,01				
9	Eleri et al., 1995	Fig. 8 SS WF	Carbonate Core R1	0,24	11,2	refined oil / synth.brine	n/a	4,55	Core CT scan, const. flowrate, different fractions
		Fig. 6 SS WF						4,55	
		Fig.6 SS OF						4,55	
		Fig. 9 SS OF						4,55	
10	Fulcher et al., 1985	run4	Berea sandstone	0,23	325,3	oil / brine100%	37,9	2,496	Constant Ca
		run8		0,23	219,7	oil / brine 60%	5,5	0,814	
		run11		0,23	365,9	oil / brine11%	0,33	0,884	
		run14		0,23	353,4	oil / brine 40%	30,3	0,171	
		run15		0,23	311,1	oil / brine 18%	29,7	0,018	
		run16		0,22	433,1	oil / water	0,04	0,950	
		run17		0,22	433,1		0,45	0,158	
		run18		0,22	416,4		2,91	0,016	
		run19		0,22	384,5		0,12	0,356	
		run20		0,23	531,6		25,9	0,002	

Table 2 (*continued*)

	Lab study	Source Ref.	pore network type	Φ	$\tilde{k}$ (md)	Fluids	$\tilde{\gamma}_{ow}$ (d/cm)	κ	Comments
				porosity	Absolute permeability	non-wetting / wetting	Interfacial tension	Viscosity ratio	
11	Geffen et al., 1951	fig.8	Nellie Bly sandstone (Alternating shales and hard gray sandstones)	0,26	482	oil (10-cane+12-cane) / brine	n/a	1,515	Effects of pressure gradient & saturation history
		fig.14							
12	Ghassemi & Pak, 2011	fig. 11	Virtual pore network, Lattice2D, chamber-and-throat type, const. 0,02mm	0,45	n/a	n-nonanol (nw) / formamide (w)	4,3 mN/m	1,00	Lattice-Boltzmann simulations
		fig. 11						1,00	
		fig. 12						3,00	
		fig. 12						3,00	
		fig.13						3,00	
		fig. 13						0,33	
		fig. 14						0,33	
		fig. 15						3,00	
13	Kleppe & Morse, 1974	Table2	Single block Berea sandstone core	0,23	290	oil / water	n/a	0,500	Study of effect matrix fracture
		fig.3	Fractured Berea sandstone core			oil / brine		2,300	
14	Lai & Miskimins, 2010	fig.4	propant pack ceramic 12/18	n/a	n/a	water / nitrogen gas	n/a	0,020	Propant packs under high confining stress conditions
		fig.5	propant pack ceramic 20/40	n/a	n/a				
15	Leverett, 1939	fig. 9	High perm unconsldtd Sand II	0,350	1750	kerosene / water		1,791	Effects of viscosity, interfacial tension & packing-
			High perm unconsldtd Sand III	0,450	1040	kerosene / water + glycerol		0,341	
16	Li et al., 2005	fig.4	Virtual homogeneous sphere pack medium (LB)	0,36	n/a	virtual wetting / non-wetting fluids	n/a	1,00	Constant Ca. Lattice-Boltzmann simulations
		fig.4						1,00	
		fig.7						1,00	
		fig.7						1,00	
		fig.8						1,45	
		fig.9						3,35	
17	Lo & Mungan, 1973	fig.4	Teflon	0,425	2400	kaydol / brine	37,61	107,30	Effect of temperature
		fig.5		0,401	1180	protol / brine	16,99		
		fig.6		0,454	2180	tetradecane / brine	20,89		
		fig.7	Berea sandstone	0,216	600	kaydol / brine	37,61		
		fig.8		0,237	560	protol / brine	16,99		
		fig.9		0,240	620	tetradecane / brine	20,89		
18	Maloney at al., 1993	fig.11 table C2, drain/ imbbtn.	Berea sandstone (Almond Formation – Patrick Draw field, Arc Unit Well 121)	0,182	5,8	Nitrogen / brine	n/a	0,02	
		fig.12 table C3, drain/ imbbtn				oil / brine		1,00	Const fractional flow
19	Masalmeh, 2003	fig.14 2nd drng	Plugs of heterogeneous matrix	0,32	3,5	crude oil / brine	0,02	5,885	Effect of wettability heterogeneity
		fig.14 1st drng					0,02	5,885	
		fig.15 2nd drng			2,1		0,02	5,885	
20	Nordtvedt et al., 1994	fig.1b	outcrop chalk	0,284	4,2	oil / water		1,085	Const flowrate
		fig.2b							
21	Oak et al., 1990	fig.4	Berea sandstone, fired	n/a	210	Gas / water	n/a	0,018	
				n/a	210	Oil / gas		0,011	
22	Odeh, 1959	fig. 6	Core sample 3, prepared from consolidated rocks cut in the direction of the bedding plane.	0,188	212,5	Oils: light naphtha, light Socony Mobil oil & two viscous mineral oils. Aqueous phase: water solution of two concentrations of NaCl (variable viscosity).	52,20	0,488	Study of the effect of viscosity ratio. Implemented the Pennsylvania State method
							53,00	0,438	
							48,50	5,756	
							49,20	5,156	
							46,40	46,744	
							47,00	41,875	
							46,40	82,907	
							47,10	74,271	
		fig. 7	Core sample 4, prepared from consolidated rocks cut in the direction of the bedding plane.	0,162	15,5		52,20	0,488	
							53,00	0,438	
							48,50	5,756	
							49,20	5,156	
							46,40	46,744	
							47,00	41,875	
							46,40	82,907	
							47,10	74,271	
23	Perrin, et al., 2009	fig. 4b	Rock plug, CO_2CRC-Otway project, AU	0,182	50	CO_2 / brine	n/a	0,074	Effect of core heterogeneity &

Table 2 (*continued*)

	Lab study	Source Ref.	pore network type	Φ	$\tilde{k}$ (md)	Fluids	$\tilde{\gamma}_{ow}$ (d/cm)	Κ	Comments
				porosity	Absolute permeability	non-wetting / wetting	Interfacial tension	Viscosity ratio	
		fig.7b 2,6ml/min	heterogeneous Berea sandstone	0,203	430			0,076	injection flowrate
		fig.7b 1,2ml/min						0,076	
24	Ramstad et al., 2012	fig.2a	water wet Bentheimer sandstone	0,219	1,9	oil / water	35,0	1,321	Laboratory measured rel-perm data
		fig.2c		0,219	1,9		35,0	1,321	
		fig.2b	water wet Berea sandstone	0,193	1,2			1,324	
		fig.2d		0,193	1,2			1,324	
						Virtual fluids	35,0	0,1	Lattice-Boltzmann simulations
								1,0	
								10,0	
25	Reynolds et al. 2014	Fig.7 q_T=7ml/min	Bentheimer sandstone core, (>95% quartz / minor feldspars and clays), simple heterogeneity, unreactive mineralogy, strongly water-wet.	0,222 ± 0,019	1810 ±120	N_2 / Brine	62,0	0,040	Const total flow
		Fig.7 q_T=7ml/min							Const total flow
		Fig.7 q_T=7ml/min							Const total flow
		Fig.7 q_w=0,675ml/min							Const Ca
		Fig.7 q_w=0,5ml/min							Const Ca
		Fig.5, Exp.2				CO_2/DI-water	36,97	0,070	Effect of interfacial tension and viscosity ratio
		Fig.5, Exp.3				CO_2 / Brine	36,92	0,071	
		Fig.5, Exp.5				CO_2-brine	34,24	0,081	
		Fig.5, Exp.6					34,00	0,080	
		Fig.5, Exp.4				CO_2/DI water	41,00	0,040	
		Fig.5, Exp.7					40,97	0,051	
26	Richardson _et al_1952	fig.12 ΔP=50-80" H_20	Berea outcrop sample			gas / oil		0,011	Comparison of rel-perm measurement techniques
		fig.12 ΔP=200" H_20							
		fig.12 ΔP=350" H_20							
27	Sandberg_et al_1958	fig. 8	Consolidated sandstone outcrop, sample 2703, Aris formation	0,278	757	oil / water		0,451	Study of the effect of flowrate and viscosity
						oil / water		1,299	
						oil / water		1,906	
28	Shafer et al., 1990	fig.2	Carbonate core	n/a	19,0	oil / water	n/a	1,860	Hybrid steady-unsteady- state technique
29	Sheng et al., 2011	fig.5	virtual (CT image of sandstone plug)	0,310	2k	virtual w / nw	53,50	1,000	Pore network modeling of rel-perm from micro-CT images
		fig.7							
30	Talash, 1976	fig.3 drainage	Fired Berea Core SFB-1	0,253	1410	Brine + .04% surfactant / crude oil	n/a	8,096	Effect of surfactant
		fig.3 imbibtn.							
		fig.4 drainage	Fired Berea Core SFB-2	0,252	1467	brine + surfactants / crude oil			
		fig.4 imbibtn.							
		fig.6 drainage							
		fig.6 imbibtn.							
31	Tsakiroglou et al., 2015	Table 1	well-sorted sand pack	0,420	25000	oil (n-C10 + n-C12) / brine	50,0	1,00	Equal viscosities, constant Ca
32	Virnovsky et al., 1995		virtual core (LB sim)	0,220	485,0	oil / water	n/a	0,815	Lattice-Boltzman simulations.
33	Virnovsky et al., 1998	fig.2	Berea sandstone	0,561	216,0	oil / water	45,82	0,866	Constant total flowrate of oil & water
				0,561	216,0				
		fig.4		0,561	216,0				
				0,561	216,0				
				0,561	216,0				
		fig.5		0,561	216,0				
				0,561	216,0				
		fig.6		0,561	216,0				
				0,561	216,0				
34	Wang, 1988	fig.3	Berea sandstone	0,185	113,0	crude / brine	n/a	3,738	Const. flowrate
		fig.4	Loudon Core L1	0,208	163,0				
		fig.15	Berea Core B1	0,183	112,0				
		fig.16	Berea Core B1	0,183	112,0				
		fig.17	Loudon Core L1	0,208	163,0				
		fig.18	Loudon Core L1	0,208	163,0				
35	Wyckoff & Botset, 1936	Fig. 5	Unconsolidated sand		17,8k	CO_2 / water	n/a	0,015	Effect of unconsolidated sand packing
		Fig. 6			44,3k				

flowrates.

- Virnovsky et al., 1995 and 1998, demonstrated the dependence of relative permeabilities on flow rates by implementing steady-state core floods at different rates spanning high (lab) rate values to low (reservoir) rate values.
- Wang, 1988, studied the effect of wettability alteration in various sandstones.
- Wyckoff and Botset, 1936, in one of the first laboratory studies of the flow of gas-liquid mixtures through unconsolidated sands, presented results for experiments on four sands of widely different permeabilities using carbon dioxide and water.

The majority of studies used in the present work span a period of 7 decades. The oldest having been published in the 1950 s (Geffen et al., 1951). The most recent is that of Tsakiroglou et al. (2015). There are many laboratory derived relative permeability diagrams published in the early decades of the 20th century but these have a historic value; they do not provide adequate variety of critical data on system/flow configurations (e.g. absolute permeability, fluid viscosities, interfacial tension, flowrates) therefore they cannot be used. The studies of Wyckoff and Botset, 1936; and Leverett, 1939, are two exceptions. A general comment is that the disclosure of information on critical operational and system parameters implemented in the studies, increases with time. For the purpose of the present retrospective examination, only those studies providing a minimum necessary information (relative peremabilities and viscosity ratio) have been selected.

We must stress here that the scope of the present work is not to provide an extensive review of laboratory studies of relative permeability but rather to provide ample experimental evidence on the existence of optimum operating conditions and reveal energy efficiency characteristics. To this end we cannot claim/warrant that the present list of studies is to be considered as either complete or exhaustive. It is expected that more studies will be traced as a result of deeper delving into literature data bases.

3.2. Data acquisition and transformation

A simple, two-step, cropping-and-matching procedure was implemented to acquire data from published relative permeability diagrams. These data were then used to derive the corresponding energy efficiency diagrams. The process is outlined in the following (with reference to Fig. 2).

3.2.1. Data cropping

Each diagram was electronically cropped from the original manuscript. Then, general purpose spreadsheet software (Valavanides, 2013) was used to construct blank relative permeability diagrams on which the original diagrams were superimposed. Proper scaling and coordinate values for (S_w, k_{ro}) and (S_w, k_{rw}),

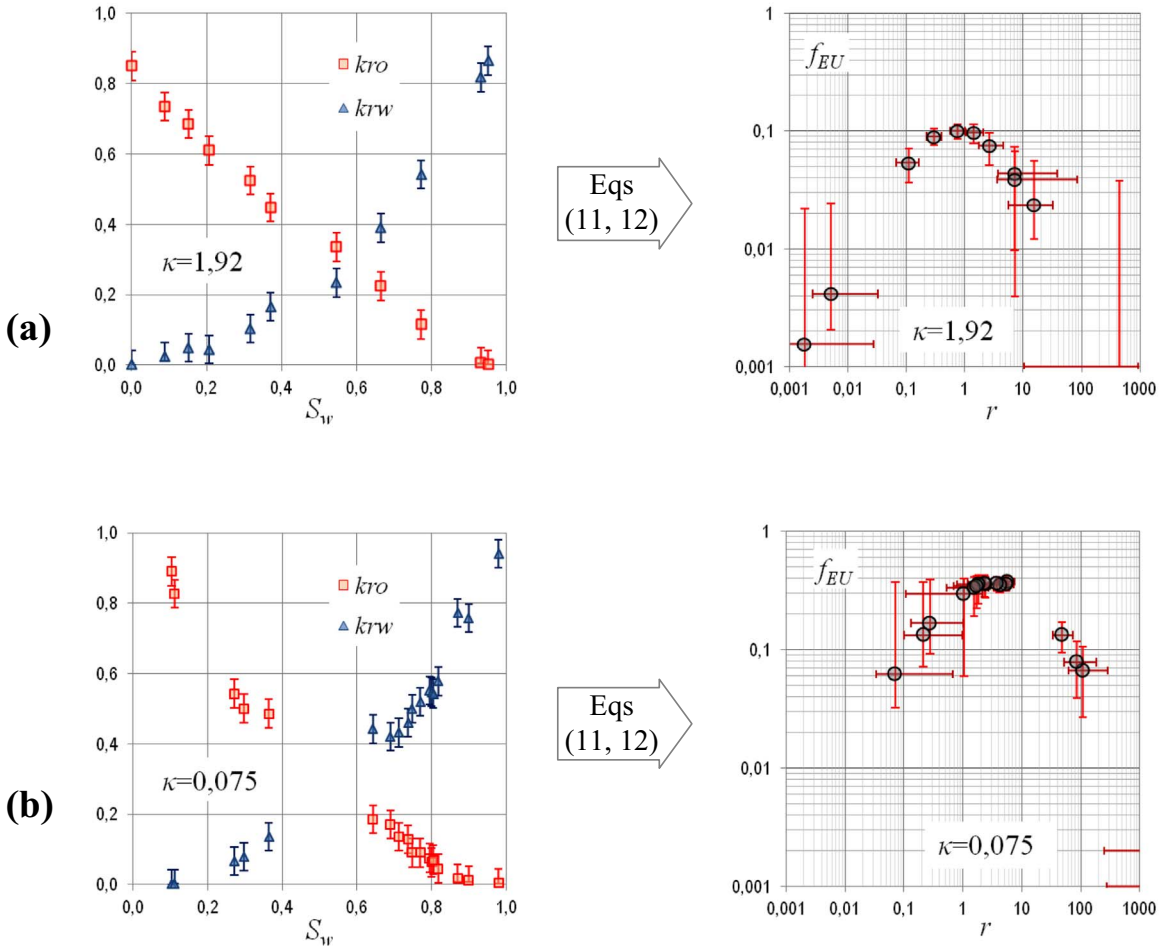

Fig. 3. Effect of the uncertainty in reading the exact value of the relative peremability values, k_{ro}, k_{rw}, on the determination of the optimum operational conditions, i.e. the maximum value of f_{EU} and its position r^*. (a) Favorable conditions $0 < \kappa < 1$ (b) Unfavorable conditions, $1 < \kappa$. Base values (□, △) are cropped from the original relative permeability diagrams in Fig. 2 (Bentsen, 2005) and then perturbed by ± 4%.

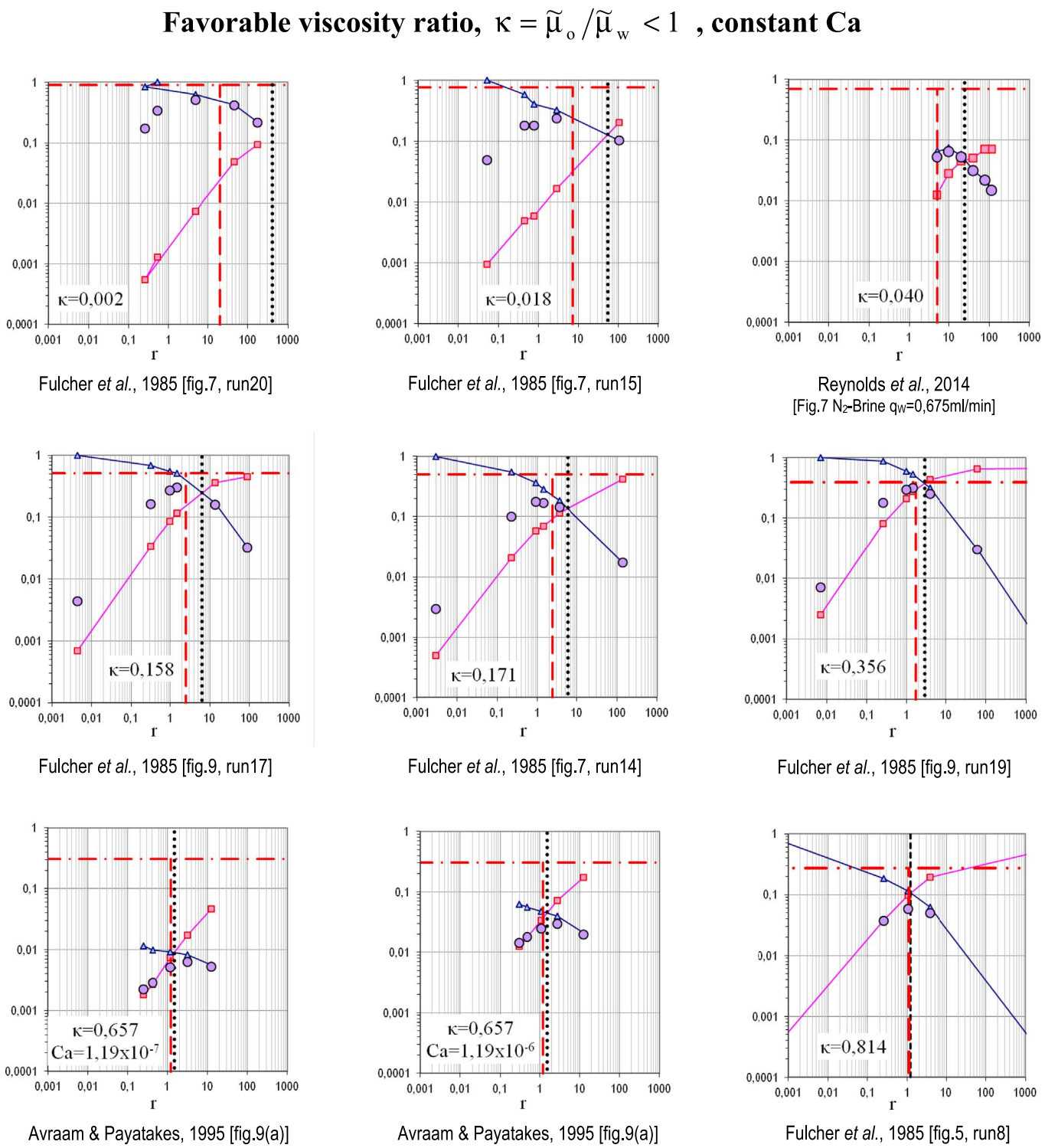

Fig. 4. Relative permeability for "oil" (□) and "water" (△) and energy utilization index, f_{EU}, (○) against flowrate ratio, r, for "oil/water" systems with favorable viscosity ratios $\kappa = \tilde{\mu}_o/\tilde{\mu}_w < 1$ and for various constant flowrate (const. Ca) conditions. Sub-legends refer source data.

were manually selected so that the respective spreadsheet markers would fit the corresponding markers of the original diagram. Other methods have been tried as well. Specifically, commercially available CAD software package was used to automatically detect marker groups and deliver their coordinates. Nevertheless, the inherent complexity in crowded markers within "dense" diagrams, or the slightly distorted or poor scan quality of older papers, proved to be a disadvantage for implementing an automatic data acquisition process, thereby human intervention was necessary. To minimize data acquisition error, a uniform consistency check was implemented after the first stage of data cropping from the original diagrams. The issue of data cropping accuracy, especially the uncertainty associated with reading low range values of relative permeability (<0, 1), is discussed in paragraphs 3.2.4.

3.2.2. *Transformation and plotting of data*

The data sets acquired from the original relative permeability

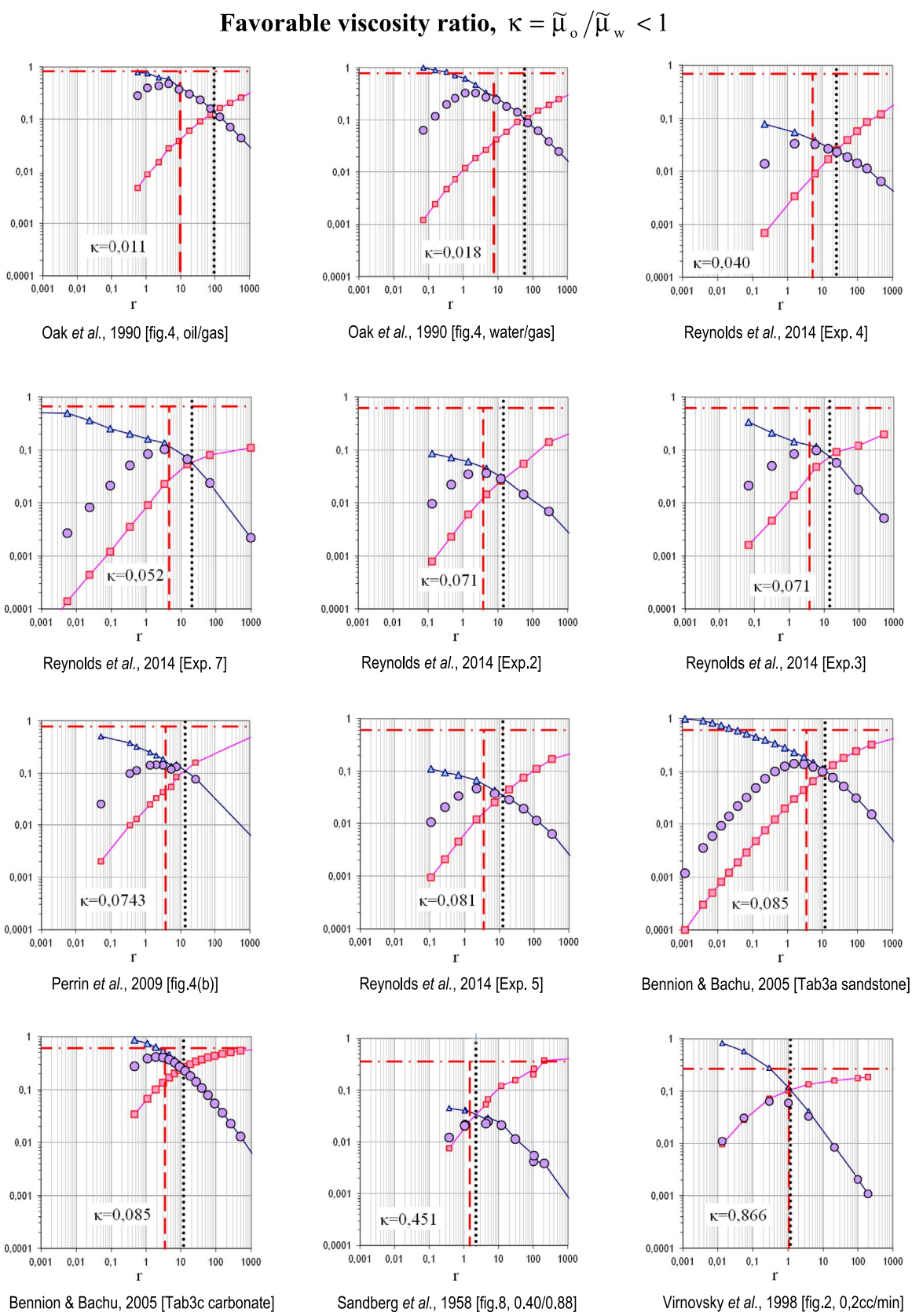

Fig. 5. Relative permeability for "oil" (□) and "water" (△) and energy utilization index, f_{EU}, (○) against flowrate ratio, r, for "oil/water" systems with favorable viscosity ratios $\kappa = \tilde{\mu}_o/\tilde{\mu}_w < 1$ and for various flow conditions. Sub-legends refer source data.

Unfavorable viscosity ratio, $1 < \kappa = \tilde{\mu}_o / \tilde{\mu}_w$, constant Ca

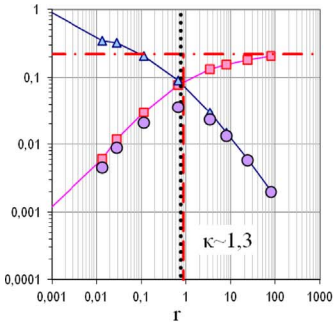

Dernaika *et al.*, 2005 [fig. 5(a) RRT1-113]

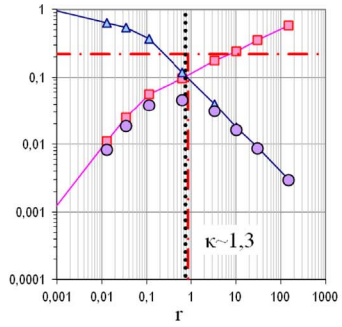

Dernaika *et al.*, 2005 [fig. 5(a) RRT2-15]

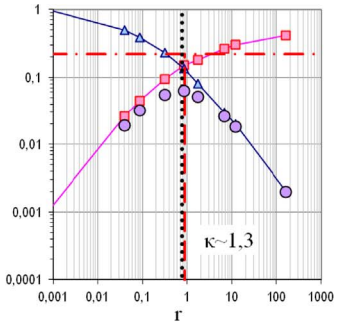

Dernaika *et al.*, 2005 [fig. 5(a) RRT3-72]

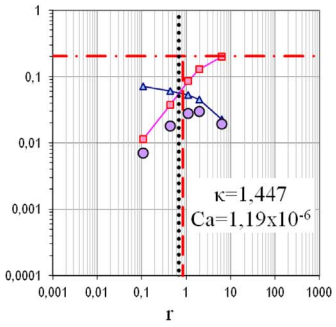

Avraam & Payatakes, 1995 [fig.9(b)]

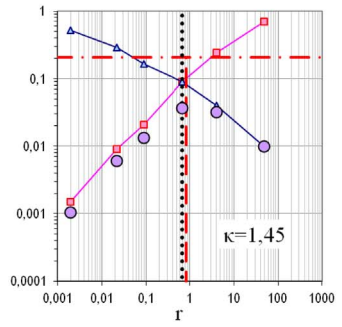

Li *et al.*, 2005 [Fig. 8]

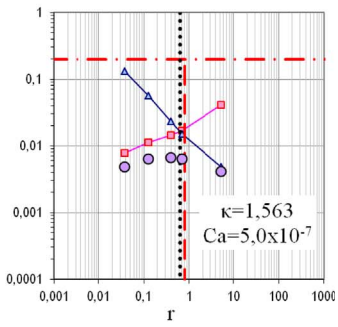

^vraam & Payatakes, 1999 [Table 3, Fluid 2]

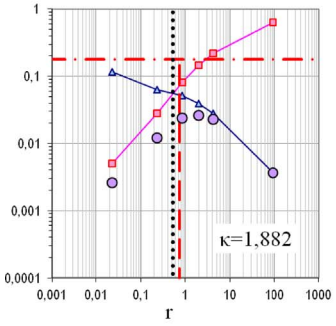

Allen & Pucket, 1986 [fig.7, run 8]

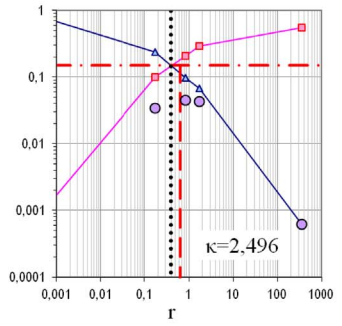

Fulcher *et al.*, 1985 [fig.4, run 4]

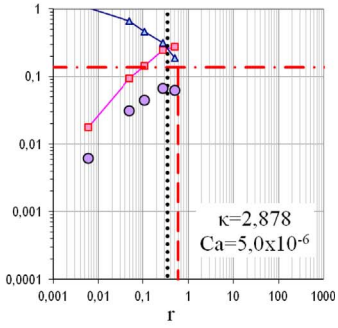

Avraam & Payatakes, 1999 [Table3, Fluid 1]

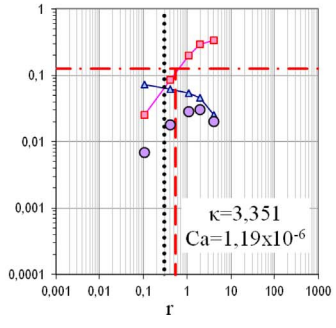

Avraam & Payatakes, 1995 [fig.9(c)]

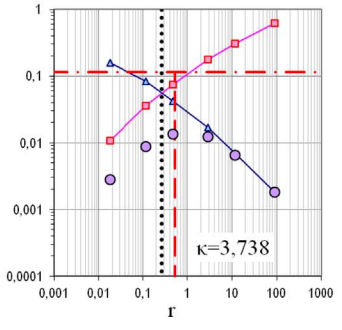

Wang, 1988 [fig.15, drainage]

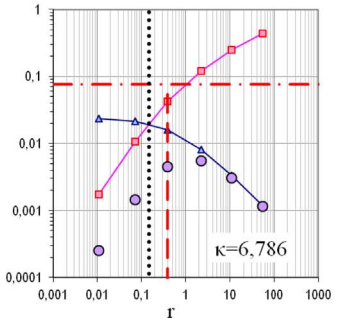

Braun & Blackwell, 1981 [fig.5]

Fig. 6. Relative permeability for "oil" (□) and "water" (△) and energy utilization index, f_{EU}, (○) against flowrate ratio, r, for "oil/water" systems with unfavorable viscosity ratios $1 < \kappa = \tilde{\mu}_o/\tilde{\mu}_w$ and for various constant water flowrate (constant Ca) conditions. Sub-legends refer source data.

Unfavorable viscosity ratio, $1 < \kappa = \tilde{\mu}_o / \tilde{\mu}_w$

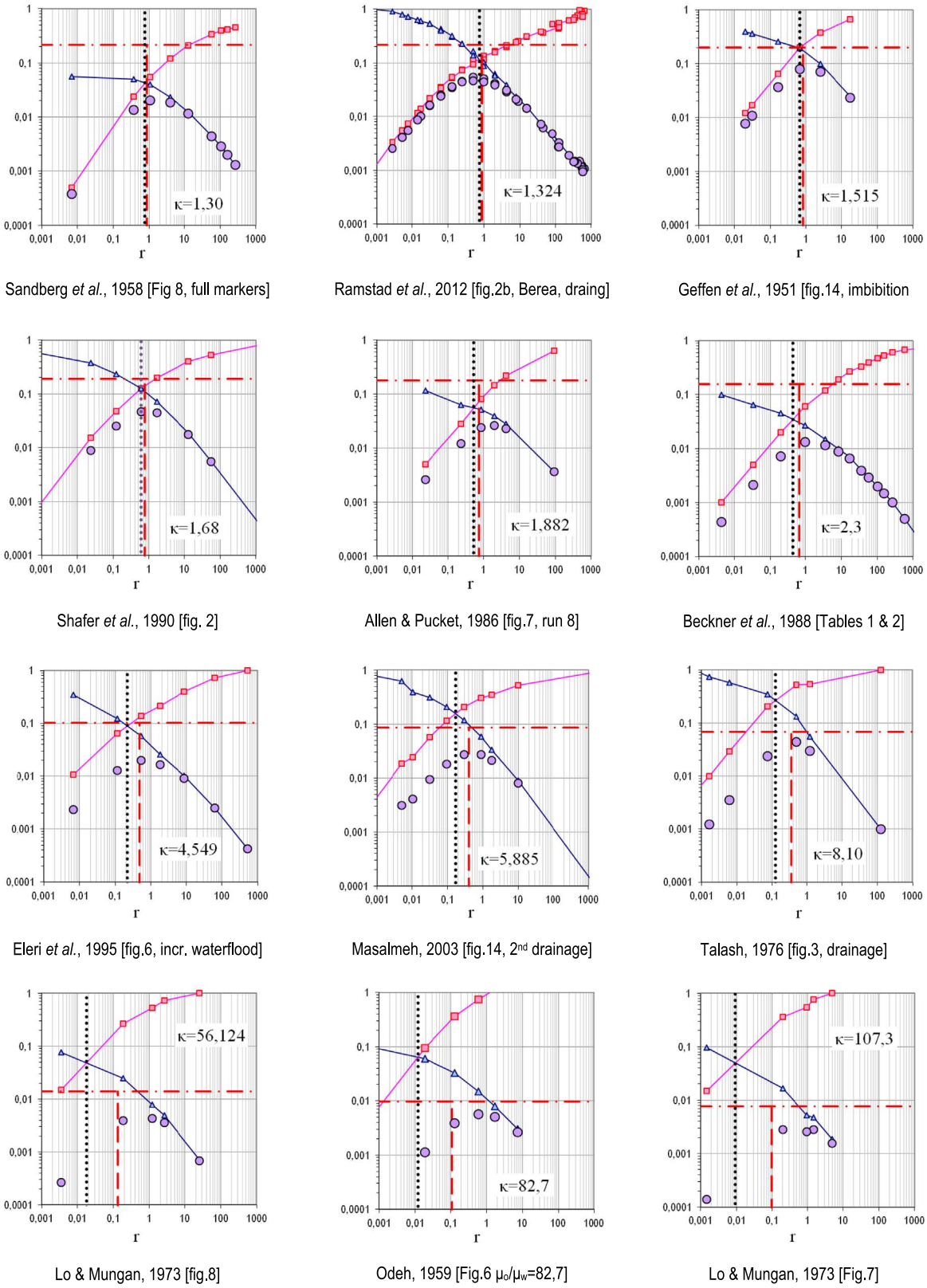

Fig. 7. Relative permeability for "oil" (□) and "water" (△) and energy utilization index, f_{EU}, (○) against flowrate ratio, r, for "oil/water" systems with unfavorable viscosity ratios $1 < \kappa = \bar{\mu}_o/\bar{\mu}_w$ and for various flow conditions. Sub-legends refer source data.

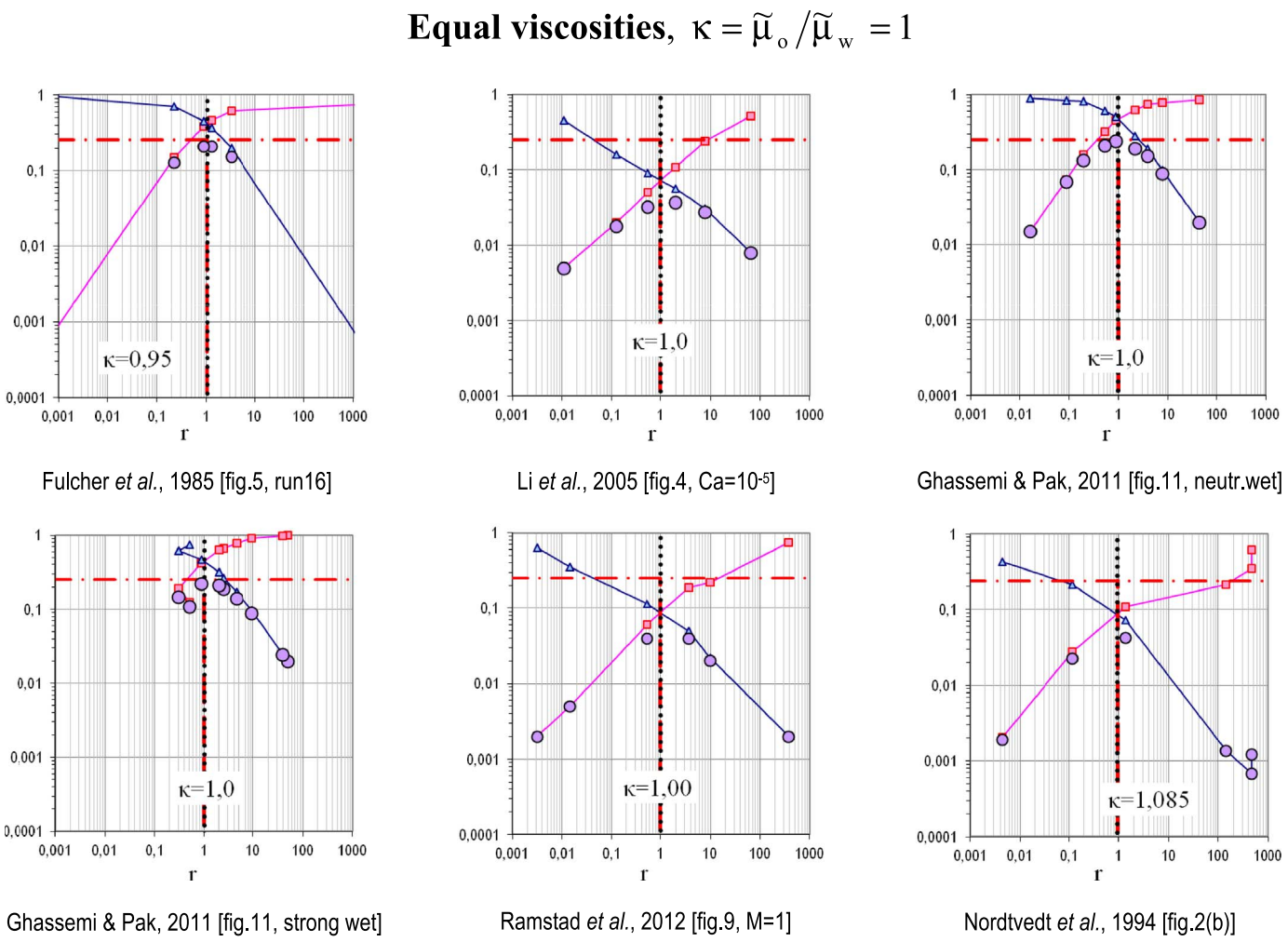

Fig. 8. Relative permeability for "oil" (□) and "water" (△) and energy utilization index, f_{EU}, (○) against flowrate ratio, r, for "oil/water" systems with equal viscosities and for various flow conditions. Note that $r_x = r^*_\infty$.

diagrams (Fig. 2, upper row), as well as critical information on the materials and methods of each study, provided the necessary input for the transformation, Eqs. (11–12). Each one of the derived operational efficiency vs flowrate ratio data sets, $\{f_{EU}, r\}$, were plotted on a new (log-log) diagram together with the seed relative permeability data (Fig. 2, middle row). Similarly, implementing Eq. (9) it is also possible to plot k_{ro}, k_{rw} and f_{EU} values against the fractional flow of oil, f_o (Fig. 2, bottom row). Markers fitted in each pair of (k_{ro}, S_w) and (k_{rw}, S_w) in the source diagrams of row (I), Fig. 2, tally with markers in the derived diagrams in rows (II) and (III). Each rectangular marker (□) indicates a source k_{ro} value and each triangular marker (△) indicates the corresponding k_{rw} value. Circular markers (○) indicate values of f_{EU}. In addition, the reconstructed diagrams (rows II and III) contain one dotted line in black and two lines in red, one vertical (dashed) and one horizontal (dash-dotted).

The vertical, dotted line in black indicates the value of the flowrate, r_x (row II) or, accordingly, the value of the oil fraction, f_{ox} (row III), for which the relative permeability value of oil and water are equal. Simply put, values r_x or f_{ox} indicate the flow conditions of the crossover point of relative permeabilities. The horizontal, dash-dotted line indicates the value of the maximum attainable energy efficiency of the particular oil-water-porous medium system, $f^*_{EU\infty}$. The vertical dashed line in red indicates the corresponding values of the flowrate ratio, r^*_∞, or oil fraction, $f^*_{o\infty}$, for which the maximum value of energy efficiency is attained. For both measures, see Section 4 "Results and Discussion".

The saturation, S_w, and the flowrate ratio, r, are -in general- inversely related, i.e. as saturation increases, flowrate ratio decreases. [Observe the coordinate values of corresponding relative permeability markers in the diagrams in Fig. 2. In particular, observe the pair of markers indicated by the arrows in the left column diagrams]. Considering the phenomenology of the process, as S_w is increased towards unity, oil saturation decreases to zero, reaching the limit of irreducible oil saturation; any small quantity of oil is broken up to small tiny oil blobs that get stranded and, practically, there is no flow of oil, therefore $r \to 0$. On the contrary, as S_w decreases to zero, the oil practically saturates the pore network, the flow of water is negligible, compared to the flow of oil, and the flowrate ratio sharply increases to very high values. The particular trend has been observed in the laboratory studies of Wyckoff and Botset, 1936 (Fig. 11) and Naar et al., 1962 (Fig. 7).

3.2.3. *Selection of the flowrate ratio, r, as independent variable*

As stated in paragraph 2.2, the flowrate ratio, r, is used as one of the two independent variables (the other being Ca). Alternatively, the fractional flow of oil, f_o, or water, f_w could be used. Switching between r and f_o (or f_w) is readily provided through Eq. 9. The implications in using f_o instead of r are presented in the bottom row diagrams of Fig. 2. In general, the domain $-3 \le \log r \le 3$ is mapped through Eq. (9a) into the domain $0{,}001 < f_o < 1{,}0$. The particular mapping is not linear. It is easy to observe that the use of f_o (or f_w) in

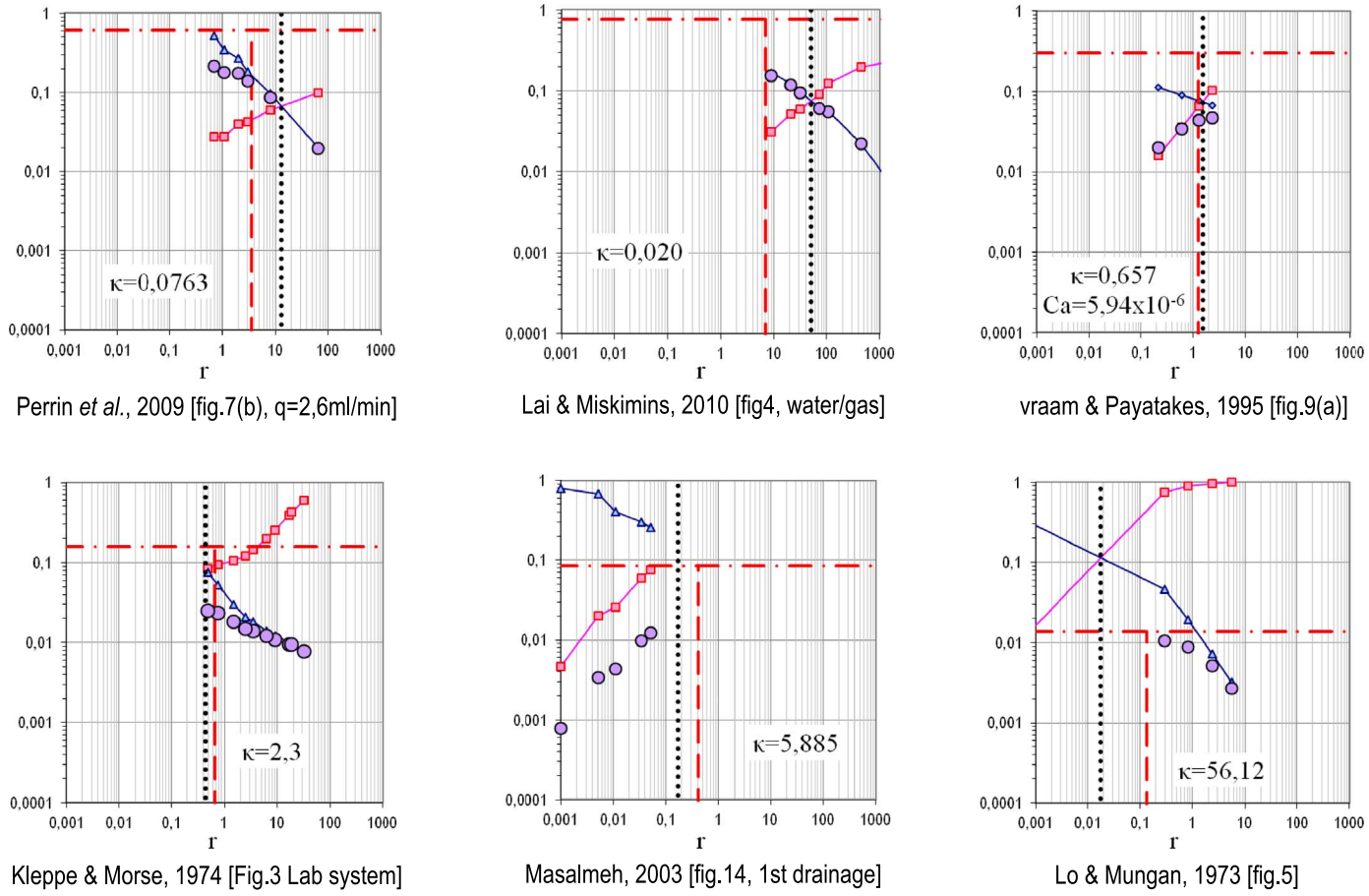

Fig. 9. Relative permeability for "oil" (□) and "water" (△) and energy utilization index, f_{EU}, (○) against flowrate ratio, r, for various "oil/water" systems and flow conditions. Sub-legends refer source data. Note that "maxf_{EU} conditions" do not appear, eventually because the pertinent flow conditions have not been reached or examined.

the abscissa provides a scale magnification in the area $< -1 <$ log$r < 1$ on the expense of a scale shrink outside that area (compare scales at the middle and bottom row diagrams, Fig. 2). One implication is that the markers are separated in the central part, whereas they crowd-up at the left and right parts of the abscissa, i.e. as f_o approaches 0 and/or 1. The decision in using r as the independent variable was based on the observation that $f_{EU}(r)$ diagrams were smoother and showed a more uniform trend irrespective of the particular values of the system parameters and flow conditions. This can be verified by an overall observation of diagrams in Figs. 4–9. In addition, it was more convenient to have a direct comparison (benchmark) with the *DeProF* predictions diagrams in Fig. 1.

3.2.4. Uncertainty in data

Because of the trend of the relative permeability values, logarithmic scales are most convenient to map the variation over the (0, 1) domain. Nevertheless, this was not the case in many of the diagrams we have collected. Therefore, we have examined the accuracy in reading the relative permeability values from the source diagrams and the effects of the associated uncertainty, especially in the low-range values on linear scale diagrams. We have contrived the following test. After considering a certain – fictitious- reading error on the source relative permeability values, we have estimated the associated uncertainty in the determination of the values of the flowrate ratio, r, and the energy utilization coefficient, f_{EU}. An indicative test is presented in the diagrams in Fig. 3. We induced a reading error of $\pm 4\%$ in the relative permeability values cropped from the original diagrams of Bentsen, 2005 (Fig. 2). This is indicated with the y-error bars in the left column diagrams of Fig. 3. Then, we have considered the 4 combinations of high and low values of the relative permeability of oil and water to estimate [through Eqs. (11, 12)] the corresponding extreme values in r and f_{EU}. These are indicated with the x- and y-error bars in the right column diagrams. It is clear that the relative error is maximized when the relative permeability values are largely different, i.e. at the range of small or large values of saturation. In the midrange values of saturation, where relative permeability values are of comparable magnitude, the relative error is minimized and the essential feature validated in the present work, the existence of optimum operating conditions, i.e. its location and measure, is insensitive at least up to the data uncertainty range we have considered ($\pm 4\%$).

It is worth noting that the effect of data *reading* uncertainty on the determination of the maximum value of f_{EU} as well as on the associated flow conditions, r^*, is negligible, or, at least, non-critical. In addition, since the source values themselves are actually measured, the last statement can be considered as equivalently true for the *measuring* uncertainty on the relative permeability values.

We close this passage with two remarks: (a) Actual reading error is much less than the trial /indicative value of $\pm 4\%$ considered here. (b) In logarithmic scale diagrams, due to the associated scaling effect, even when relative permeability values are considered in the range $0{,}01 < k_{ri} < 0{,}001$, a *reading* error of 4% is essentially mapped as an *actual* or *effective* error $< 0{,}04\%$.

4. Results and discussion

A collection of the most representative diagrams is presented in Figs. 2 and 4–9. Due to space limitations, it was impossible to present in detail all the 179 transformed diagrams. The interested reader may refer to a technical report (Valavanides et al., 2015b), containing all the source diagrams of the original studies, the extracted data values, as well as the new diagrams produced from the transformed data. The source material (relative permeability diagrams) will be augmented in the future as more studies will be detected. As referenced in the Introduction, intention is to build a tentative data base of laboratory studies. In all of the diagrams (Figs. 2, 4–9 and Valavanides et al., 2015b) the following trends are observed.

4.1. Existence of maximum energy efficiency conditions

Every set of $\{f_{EU}, \log r\}$ values, corresponding - through transformation (11 – 12)- to a $\{k_{ro}, k_{rw}\}$ data set, presents a maximum. Considering the number and diversity of the examined relative permeability diagrams, there is adequate proof of the *existence* of a locus of optimum operating conditions in steady state two-phase flow in porous media, as first indicated /predicted by the *DeProF* model. Diagrams pertaining to constant *Ca* flow conditions (Allen and Pucket, 1986; Avraam and Payatakes, 1995, 1999; Braun and Blackwell, 1981; Dernaika et al., 2012; Eleri et al., 1995; Fulcher et al., 1985; Li et al., 2005; Reynolds et al., 2014; Tsakiroglou et al., 2015; Virnovsky et al., 1998; Wang, 1988, presented in Figs. 4 and 6 and/or in Valavanides et al., 2015b) show a trend typical to the trend of the *DeProF* model predictions (Fig. 1): $f_{EU}(Ca,r)$, for constant *Ca*, attains a skewed-to-the-right bell-shaped form as it progressively increases -with increasing logr- towards a maximum value at $\log r^*$, and then, sharply decreases, as logr approaches a limiting value -above which two-phase flow is not any more physically sustainable. The aforementioned relative permeability diagrams would provide a better benchmark to the *DeProF* model predictions if they contained more data points (more relative permeability measurements). Many of the produced $f_{EU}(\log r)$ diagrams appear as slice-cuts or, better, curved-slice-cuts obtained from a plane cut (i.e. at constant *Ca* value) of some general form of surface diagrams similar to the $f_{EU}(Ca, \log r)$ diagrams predicted by the *DeProF* model (Fig. 1). This is so because the majority of the relative permeability diagrams are furnishing steady-state permeability measurements over different values of the capillary number, therefore, getting a plane cut is not always possible.

We must stress here that we detected a few exceptional cases where, presumably, the original laboratory measurements were taken over a narrow span of flow conditions and, therefore, optimum operating conditions have not been reached. Such indicative cases are presented in Fig. 9.

Depending on the imposed flow conditions, the operational efficiency of the process may change significantly, even by two orders of magnitude. There are no peaks or abrupt changes in f_{EU} with changes in r (in all diagrams) and max f_{EU} can be reached in a smooth and continuous manner. Both attributes are of paramount importance when process efficiency is considered for industrial scale applications.

4.2. Crossover point of relative permeabilities

A critical process characteristic can be identified by observing the critical value of the flowrate ratio for which the relative permeability of oil and water become equal, commonly referred to as, the crossover point of relative permeabilities. Following a careful inspection of all diagrams, it appears that, *systematically*, the value of r_x, indicated by the vertical, dotted black line, is exactly equal to the inverse of the viscosity ratio, i.e. $r_x = \kappa^{-1} = (\bar{\mu}_o/\bar{\mu}_w)^{-1}$. There is no such indication as of any dependence other than the viscosity ratio. This can be verified analytically through Eq. (11) by setting $k_{ro} = k_{rw}$. The feature indicates that the viscosity ratio is a critical system parameter of the sought process.

4.3. Maximum efficiency conditions versus crossover point of relative permeabilities

Another interesting feature can be revealed by observing the diagrams in the middle row of Fig. 2. Both are produced from the same study, with the same type of porous medium and following the same protocol, albeit different fluid properties (viscosity ratio) and different flow conditions were implemented. A comparative observation of the energy utilization diagrams will reveal that the discrepancy between r_x (the crossover point of relative permeabilities) and r^* (where local maximum operational efficiency is attained) depends on the system setting and flow conditions. This feature can also be identified over all energy utilization diagrams in Figs. 4–7. Specifically, in systems with favorable viscosity ratios ($\kappa < 1$), $r^* < r_x$, whereas in systems with unfavorable viscosity ratios ($1 < \kappa$), $r_x < r^*$. The "distance" between these two figures, $|r^* - r_x|$, seem to correlate to the values of the system parameters and the imposed flow conditions. In cases where the system comprises fluids of equal viscosity ($\kappa = 1$), the flowrate values for which maximum operational efficiency is attained, coincide with those pertaining to equal permeabilities, i.e. $r^* = r_x$.

The correlation between the distance $|r^* - r_x|$, the flow conditions and the values of the system parameters needs further investigation.

4.4. Effect of viscosity ratio

Consider now the discrepancy between the relative permeability, k_{ro}, k_{rw}, and the energy utilization values, f_{EU}, for any flow condition (Ca, r). Careful observation of this discrepancy across the set of diagrams in Figs. 4–8, will reveal that the discrepancy seems to be correlated to: (a) the magnitude of the viscosity ratio, (b) the "distance" of the flow conditions, r, from r^*. The observed trend is that, as the disparity between the viscosities of the two fluids is reduced, i.e. as $|\kappa - 1| \to 0$, the effect of the distance $|r - r^*|$ becomes less significant, i.e. the discrepancy between relative permeability and energy utilization values is reduced and extends over a broader range of the flowrate ratio domain.

This systematic trend is in compliance with laboratory studies (Vizika et al., 1994) showing that the extent of mobilization of the disconnected oil and the residual oil saturation following a water flood (imbibition), depend not only on the capillary number but on the *combined* effect of the oil/water viscosity ratio and the capillary number. Extending the conclusions of the study, one can imply that there must be favorable combinations of the capillary number and the viscosity ratio values whereby the system is "tuned" to significant mobilization of disconnected oil blobs. The result of the tuning is that the flowrate of oil is maximized for the mechanical power input to the pumps and, consequently, f_{EU} takes locally maximum values.

4.5. Maximum attainable efficiency

A critical value of the energy efficiency of the process, corresponding to pure viscous flow conditions, as $Ca \to \infty$, is given by $f^*_{EU\infty} = (1 + \sqrt{\kappa})^{-2}$. This is depicted in all energy efficiency diagrams by the dash-dotted horizontal line (in red). This critical value can be used as a measure of the maximum attainable energy efficiency for each particular oil-water-p.m. system (Valavanides, 2014). We

must stress here that the two f_{EU} maxima should not be misinterpreted as one. The value $\max f_{EU}=f_{EU}(Ca, r^*)$ pertains to the "local" maximum energy efficiency of the process, occurring when the particular oil-water-porous medium *system* is set to operate in the particular *flow* conditions, *Ca* & r^*. In contrast, $f^*_{EU\infty}$ indicates (or, is defined as) the maximum, globally attainable energy efficiency of the particular oil-water-porous medium *system*, as $Ca\rightarrow\infty$ and the flow inhibitive effect of oil-water interfaces becomes insignificant when compared to that of bulk viscosity.

4.6. Flow characterization: capillarity vs viscosity

Consider a *flow set-up* for which $f_{EU}(Ca, r^*)$ is *measured* to be "close enough" to the $f^*_{EU\infty}$ *system-set* value. In such case, the process operates close to its maximum attainable efficiency, the effect of the interfaces is drastically reduced -compared to viscosity- and the flow can be characterized as viscous. Accordingly, if a measured $\max f_{EU}$ value is "reduced-enough" (compared to the $f^*_{EU\infty}$ value), the flow is characterized as capillary dominated. Focusing once more on the two sets of diagrams in Fig. 2, one can speculate that diagram 2(a) corresponds to capillary dominated flow conditions, whereas diagram 2(b) corresponds to viscosity dominated flow conditions, as it is relatively "closer" to the "ceiling" of maximum attainable efficiency for the particular system. To support this statement we need to evaluate the ratio $\left[f^*_{EU\infty}-f_{EU}(r^*)\right]/f^*_{EU\infty}$. The maximum value of the energy efficiency reached in diagram in Fig. 2(a), pertaining to $\kappa = 0,075$, is equal to 0,38, therefore, the examined ratio attains a value $[0, 62 - 0, 38]/0, 62 = 0, 39$. In the diagram in Fig. 2(b), pertaining to $\kappa = 1, 92$, the energy efficiency reaches the value 0,10 and the same ratio shifts to $[0, 18 - 0, 10]/0, 18 = 0, 43$, indicating a more efficient process.

In general, the distance between r_x and r^* seems to be systematically correlated to the character (capillary/viscous) of the flow. As the flow conditions change from "relatively small" to "relatively large" values of superficial velocity of water, i.e. from low to high *Ca* values, the effect of interfaces becomes less pronounced (when compared to the effect of viscosity) and the character of the flow shifts from "capillarity-dominated" to "viscosity-dominated". Consider any flow, described by the set of measured values {*Ca*, *r*, f_{EU}}. According to the findings of this work (Section 4.1), for the particular value of the capillary number, *Ca*, a specific flowrate ratio value, $r^*(Ca)$ sets the process at it maximum energy efficiency, $f_{EU}(r^*)$. In that context, the flow could be characterized, e.g. as to the predominance of capillarity or viscosity, against two reference sets, the $\{r^*(Ca), f_{EU}(r^*)\}$ set, defined by the efficiency attained at the particular flow conditions, and the oil-water-porous medium system defined set, $\{r_x, r^*_\infty, f^*_{EU\infty}\}$.

Overall, the trend of the measured values of (r, f_{EU}) corresponding to (k_{rw}, k_{ro}) is remarkably similar to the trend of the $f_{EU}(Ca,r)$ values predicted by the *DeProF* model/algorithm. The evidence provided herewith supports the universality of the *DeProF* theory findings with respect to the existence of optimum operating conditions and reveals an opportunity for a deeper understanding of the physics of steady-state two-phase flow in porous media.

5. Conclusions and perspectives

The hypothesis on the existence of steady-state flow conditions, for which the energy efficiency of two-phase flow in porous media processes attains a maximum value, has been tested against publicly available laboratory data. Critical process characteristics have also been revealed. The energy efficiency of the process is considered with respect to the oil transport over the mechanical power supplied to it (or, "oil produced per kW of mechanical power dissipated in pumps"), appropriately reduced to a dimensionless variable, namely the energy utilization factor.

A total of 179 relative permeability diagrams, from 35 published laboratory studies, pertaining to a variety of steady-state two-phase flow conditions and types of porous media provided the source data. Sets of paired relative permeability values, $\{k_{ro}\}$ and $\{k_{rw}\}$, extracted from the source diagrams, were transformed to corresponding sets of flowrate ratio and energy utilization values, $\{f_{EU}, r\}$. For each conventional relative permeability diagram, a corresponding operational efficiency diagram comprising the energy utilization as well as the source relative permeabilities against the oil/water flowrate ratio was delivered.

In all the examined relative permeability diagrams, a maximum value of the process energy utilization was observed. The observed maximum was local, in the sense that it pertained to the particular set of flow conditions for the examined system. In addition, the following critical process characteristics have been observed.

The relative permeability of oil and water become equal at a flowrate value equal to the inverse of the viscosity ratio of the two phases. The energy efficiency of the process has an upper limit, inversely related to the viscosity ratio and corresponding to pure viscous flow conditions, i.e. at the high-end of the flow regime $(Ca\rightarrow\infty)$.

The uncertainty associated with the measurement of relative permeability, vis-à-vis the determination of the flow conditions for which the maximum value of the process operational efficiency is attained, is non-critical.

Optimum operating conditions, r*, seem to depend primarily on the viscosity ratio, κ, and the flow conditions, *Ca*. The effect of other physicochemical parameters, e.g. wettability, porous medium structure, etc., cannot be evaluated at this stage, because of sparsely available experimental data.

The number of studies and diagrams that were examined, as well as their diversity in terms of system and flow conditions, provide extensive laboratory proof of the validity/correctness of the *DeProF* theory predictions with respect to the existence of a system-dependent locus of optimum operating conditions, $r^*(Ca)$, and the overall trend of the energy utilization factor, f_{EU}.

The trends described in Section 4 imply that a universal law may be furnished to describe the energy efficiency of the sought process in terms of a set of pertinent flow and system parameters. The conditions whereby process efficiency attains a maximum value and its correlation with the process characteristics (oil-water-porous medium system properties and flow conditions) merit a systematic investigation. The same trends also imply that it is possible to characterize the flow, as to its capillary or viscous character, based on a few appropriately selected, non-dimensional physical variables. To understand and evaluate their effect, or reveal the underlying functional dependence, an extensive and systematic laboratory study should be designed and deployed.

Concluding, two-phase flow in p.m. is "burdened" with two factors that restrain or inhibit -to a certain extent- the superficial transport of oil and water: (a) oil disconnection and capillarity effects, (b) the bulk phase viscosities of oil and water. The former predominates within the low-end of the flow regime whereas the latter within the high-end of the flow regime. There is ample experimental evidence on the existence of certain, critical flow conditions within any particular porous medium structure, for which the combined effect of those two inhibiting factors is minimized and, hence, the efficiency of the process becomes maximum. Process engineers can take advantage of that natural intrinsic characteristic and judge where to set the balance between capillarity or viscosity. The reward will be the increase -even by order of magnitude- of the process efficiency.

Acknowledgements

This research work has been co-funded by the European Union (European Social Fund) and Greek national resources in the frameworks of the "Archimedes III: Funding of Research Groups in TEI of Athens" (MIS 379389) a RTD project (M.S. Valavanides), and, the "Vocational Education of TEI of Athens Students" (MIS299967) a stage/vocational education project (E. Totaj), of the "Education & Lifelong Learning" Operational Program.

Valuable remarks and constructive comments from anonymous referees are also gratefully acknowledged.

Appendix

The definition of oil-water flowrate ratio, r, Eq. (7) when combined with the Darcy fractional flow Eq. (1),

$$\tilde{U}_o = \frac{\tilde{q}_o}{\tilde{A}} = \frac{\tilde{k}}{\tilde{\mu}_o} k_{ro} \frac{\partial \tilde{p}}{\partial \tilde{z}} \qquad \tilde{U}_w = \frac{\tilde{q}_w}{\tilde{A}} = \frac{\tilde{k}}{\tilde{\mu}_w} k_{rw} \frac{\partial \tilde{p}}{\partial \tilde{z}} \tag{A.1}$$

and, the experimentally verified condition that in steady-state two-phase fully-developed flow conditions the pressure gradient is the same for both fluids [see Eqs. (10) and (11) and Fig. 1 in Avraam and Payatakes, 1999],

$$\left.\frac{\Delta \tilde{p}}{\Delta \tilde{z}}\right|_o = \left.\frac{\Delta \tilde{p}}{\Delta \tilde{z}}\right|_w = \frac{\Delta \tilde{p}}{\Delta \tilde{z}} \tag{A.2}$$

yields the following relation [Eq. (11)]

$$r = \frac{\tilde{q}_o}{\tilde{q}_w} = \frac{\tilde{U}_o}{\tilde{U}_w} = \frac{k_{ro}/\tilde{\mu}_o}{k_{rw}/\tilde{\mu}_w} = \frac{1}{\kappa}\frac{k_{ro}}{k_{rw}} \tag{A.3}$$

Let $\tilde{W}^{1\Phi}$ be the specific mechanical power dissipation (specific as per unit porous medium volume –p.u.v.p.m.) for one-phase flow of water at an equivalent flowrate, $\tilde{q}_w$, against a porous medium cross section of surface, $\tilde{A}$, and along a distance, $\Delta\tilde{z}$, given by

$$\tilde{W}^{1\Phi} = \frac{\tilde{q}_w \Delta \tilde{p}}{\tilde{A}\Delta\tilde{z}} = \frac{\tilde{q}_w}{\tilde{A}}\frac{\Delta\tilde{p}}{\Delta\tilde{z}} = \tilde{U}_w \frac{\tilde{\mu}_w}{\tilde{k}} \tilde{U}_w = \frac{\tilde{\mu}_w}{\tilde{k}} \left(\frac{\tilde{\mu}_w \tilde{U}_w}{\tilde{\gamma}_{ow}} \frac{\tilde{\gamma}_{ow}}{\tilde{\mu}_w}\right)^2 = \frac{(Ca\tilde{\gamma}_{ow})^2}{\tilde{\mu}_w \tilde{k}} \tag{A.4}$$

The specific (p.u.v.p.m.) mechanical power dissipation for the steady-state concurrent two-phase flow of oil and water, at flowrates $\tilde{q}_o$ & $\tilde{q}_w$ and with superficial velocities, $\tilde{U}_o$ & $\tilde{U}_w$, within a porous medium cross section of surface, $\tilde{A}$, and along a distance, $\Delta\tilde{z}$, is given by

$$\begin{aligned}
\tilde{W} &= \frac{\tilde{q}_o \Delta\tilde{p}_o + \tilde{q}_w \Delta\tilde{p}_w}{\tilde{A}\Delta\tilde{z}} = \frac{\tilde{q}_o}{\tilde{A}}\frac{\Delta\tilde{p}}{\Delta\tilde{z}}\bigg|_o + \frac{\tilde{q}_w}{\tilde{A}}\frac{\Delta\tilde{p}}{\Delta\tilde{z}}\bigg|_w \\
&= \tilde{U}_o \frac{\tilde{\mu}_o}{\tilde{k} k_{ro}} \tilde{U}_o + \tilde{U}_w \frac{\tilde{\mu}_w}{\tilde{k} k_{rw}} \tilde{U}_w = \tilde{U}_w{}^2 \frac{\tilde{\mu}_w}{\tilde{k}} \left(r^2 \frac{\kappa}{k_{ro}} + \frac{1}{k_{rw}}\right) \\
&= \frac{(Ca\tilde{\gamma}_{ow})^2}{\tilde{\mu}_w \tilde{k}} \frac{1}{k_{ro}} \left(r^2\kappa + \frac{k_{ro}}{k_{rw}}\right) = \frac{(Ca\tilde{\gamma}_{ow})^2}{\tilde{\mu}_w \tilde{k}} \kappa r \frac{1}{k_{ro}} (r+1) \\
&= \frac{(Ca\tilde{\gamma}_{ow})^2}{\tilde{\mu}_w \tilde{k}} \frac{1}{k_{rw}} (r+1)
\end{aligned} \tag{A.5}$$

Therefore, the reduced mechanical power dissipation for the steady-state two-phase flow of oil and water, W, may be expressed –elegantly- in any of the three equivalent forms

$$W = \frac{\tilde{W}}{\tilde{W}^{1\Phi}} = \frac{1}{k_{ro}} \left(r^2\kappa + \frac{k_{ro}}{k_{rw}}\right) = \kappa r \frac{1}{k_{ro}} (r+1) = \frac{1}{k_{rw}} (r+1) \tag{A.6}$$

and may be expressed in any of the following three equivalent forms, Eq. (12),

$$f_{EU} = \frac{r}{W} = \frac{k_{ro}}{\kappa(r+1)} = k_{rw} \frac{r}{r+1} = k_{ro} \left(\frac{k_{ro}}{k_{rw}} + \kappa\right)^{-1} \tag{A.7}$$

References

Allen, F.R., Pucket, D.A., 1986. Theoretical and experimental studies of rate-dependent two-phase immiscible flow. SPE10972, AEE Winfrith, Dorset, U. K., 62–74.

Alvarado, V., Manrique, E., 2010. Enhanced Oil Recovery: An Update Review. Energies 3 (9), 1529–1575. http://dx.doi.org/10.3390/en3091529.

Avraam, D.G., Payatakes, A.C., 1995. Flow Regimes and Relative Permeabilities during Steady-State Two-Phase Flow in Porous Media. J. Fluid Mech. 293, 207–236.

Avraam, D.G., Payatakes, A.C., 1999. Flow Mechanisms, Relative Permeabilities and Coupling Effects in Steady-State Two-Phase Flow in Porous Media. Case of Strong Wettability. Ind. Eng. Chem. Res. 38, 778–786.

Bazylak, A., 2009. Liquid water visualization in PEM fuel cells: A review. Int. J. Hydrog. Energy 34 (9), 3845–3857.

Beckner, B. L., Firoozabadi, A., Aziz, K., 1988. Modeling transverse imbibition in double-porosity simulators, SPE 17414, California Regional Meeting, Long Beach, California, 23– 25 March, pp. 155–169.

Bennion, B., Bachu, S., 2005. Relative Permeability Characteristics for Supercritical CO2 Displacing Water in a Variety of Potential Sequestration Zones in the Western Canada Sedimentary Basin. Society of Petroleum Engineers, SPE ATCE 2005, SPE 95547, 1-15.

Bentsen, R.G., 2005. Interfacial Coupling in Vertical, Two-Phase Flow Through Porous Media. J. Pet. Sci. Technol. 23, 1341–1380.

Burnside, N.M., Naylor, M., 2014. Review and implications of relative permeability of CO2/brine systems and residual trapping of CO_2. Int. J. Greenh. Gas. Control 23, 1–11.

Braun, E.M., Blackwell, R.J., 1981. A steady-state technique for measuring oil-water relative permeability curves at reservoir conditions. SPE 10155, 1–10.

Charpentier, J.-C., 2007. In the frame of globalization and sustainability, process intensification, a path to the future of chemical and process engineering (molecules into money). Chem. Eng. J. 134, 84–92. http://dx.doi.org/10.1016/j.cej.2007.03.084.

Clayton, S., 2014 Keynote lecture, Rock & Fluid Physics: Academic and Industrial Perspectives, Shell Technology Centre Amsterdam, NL, September 15-18.

Cushman, J.H., 1997. The physics of fluids in hierarchical porous media: Angstroms to Miles. Kluwer; Theory and Applications of Transport in Porous Media, 10. ISBN: 0792347420, 467p.

Dernaika, M.R., Basioni, M.A., Dawoud, A., Kalam, M.Z., Skjaeveland, S.M., 2012. Variations in Bounding and Scanning Relative Permeability Curves with Different Carbonate Rock Types. SPE 162215, ADIPEC 2012, AbuDhabi, U.A.E., Nov. 11–14, 1–24.

Eleri, O.O., Graue, A., Skauge, A., 1995. Steady-state and unsteady-state two-phase relative permeability hysteresis and measurements of three-phase relative permeabilities using imaging techniques. University of Bergen, Norway, pp. 643–653.

Erpelding, M., Sinha, S., Tallakstad, K.T., Hansen, A., Flekkøy, E.G., Maløy, K.J., 2013. History independence of steady state in simultaneous two-phase flow through two-dimensional porous media. Phys. Rev. E 88, 053004. http://dx.doi.org/10.1103/PhysRevE.88.

Fulcher, R.A., Ertekin, T., Stahl, C.D., 1985. Effect of capillary number and its constituents on two-phase relative permeability curves. J. Pet. Technol. 37, 249–260.

Geffen, T.M., Owens, W.W., Parish, D.R., Morse, R.A., 1951. Experimental Investigation of Factors Affecting Laboratory Relative Peremability Measurements. SPE-951099-G, Pet. Trans. AIME 192, 99–110.

Georgiadis, A., Berg, S., Makurat, A., Maitland, G., Ott, H., 2013. Pore-scale micro-computed-tomography imaging: Nonwetting-phase cluster-size distribution during drainage and imbibitions. Phys. Rev. E 88 (033002), 1–9. http://dx.doi.org/10.1103/PhysRevE.88.033002.

Ghassemi, A., Pak, A., 2011. Numerical study of factors influencing relative permeabilities of two immiscible fluids flowing through porous media using lattice Botzmann method. J. Pet. Sci. Eng. 77, 135–145.

Honarpour, M., Koederitz, L., Harvey, A.H., 1986. Relative Permeability of Petroleum Reservoirs. CRC Press, Boca Raton, Florida, USA, ISBN 0–8493–5739-X.

Khan, F.I., Husain, T., Hejazi, R., 2004. An overview and analysis of site remediation technologies. J. Environ. Manag. 71, 95–122.

Kleppe, J., Morse, R.A., 1974. Oil Production from Fractured Reservoirs by Water Displacement. SPE 5084, 49th SPE Annual Meeting, Houston, Texas, 1–20.

Lai, B., Miskimins, J., 2010. A new technique for accurately measuring two-phase relative permeability under non-Darcy flow conditions. SPE 134501, ATCE2010, Florence, Italy, 1–14.

Lake, L.W., 1989. Enhanced Oil Recovery. Prentice-Hall, Englewood Cliffs, NJ.

Leverett, M.C., 1939. Flow of oil-water mixtures through unconsolidated sands. Trans. AIME 132 (1), 149–171.

Li, H., Pan, C., Miller, C.T., 2005. Pore-scale investigation of viscous coupling effects for two-phase flow in porous media. Phys. Rev. E 72 (26705), 1–14.

Lo, H.Y., Mungan, N., 1973. Effect of temperature on water-oil relative permeabilities in oil-wet and water-wet systems. SPE 4505 Dallas, Texas, 1–12.

Maloney, D., Doggett, K., Brinkmeyer, A., 1993. Special core analyses and relative permeability measurements on almond formation reservoir rocks. NIPER 648, 1–30.
Masalmeh, S.K., 2003. The effect of wettability heterogeneity on capillary pressure and relative permeability. J. Pet. Sci. Eng. 39, 399–408.
Müller, N., 2011. Supercritical CO_2-Brine Relative Permeability Experiments in Reservoir Rocks—Literature Review and Recommendations. Transp. Porous Media 87, 367–383. http://dx.doi.org/10.1007/s11242-010-9689-2.
Naar, J., Wygal, R.J., Henderson, J.H., 1962. Imbibition Relative Permeability in Unconsolidated Porous Media. Soc. Pet. Eng. J., 13–17. http://dx.doi.org/10.2118/213-PA.
Nordtvedt, J.E., Urkedal, H., Watson, A.T., Ebeloft, E., Kolltveit, K., Langaas, K., Oxnevad, I.E.I., 1994. "Estimation of relative permeability and capilary pressure functions using transient and equilibrium data from steady-state experiments" SCA 9418 Annual Symposium of the Society of Core Analysts, 197–206.
Oak, M.J., Baker, L.E., Thomas, D.C., 1990. Three-phase relative permeability of berea sandstone. J. Pet. Technol. 42, 1054–1061.
Odeh, A.S., 1959. Effect of Viscosity Ratio on Relative Permeability. Pet. Trans. AIME Vol. 216, 346–353.
Payatakes, A.C., Constantinides, G.N., Valavanides, M.S., 1998. "Hierarchical Theoretical Models: An Informal Introduction", in Mathematical Methods in Scattering Theory and Biomedical Technology, Dassios G. et al. (eds), Pitman Research Notes in Mathematics Series, No. 390, pp. 158–169, Addison Wesley Longman Ltd, ISBN 0582368049.
Perez-Mercader, J, 2004. "Coarse-Graining, Scaling, and Hierarchies" in Non-extensive entropy: interdisciplinary applications, Santa-Fe Institute studies in the science of complexity, eds. Murray Gell-Mann, Constantino Tsallis ISBN 0-19-515976-4, Oxford University Press.
Perrin, J.-C., Krause, M., Kuo, C.-W., Miljkovic, L., Charob, E., Benson, S.M., 2009. Core-scale experimental study of relative permeability properties of CO2 and brine in reservoir rocks. Energy Procedia 1, 3515–3522.
Ramstad, T., Idowu, N., Nardi, C., Oren, P.E., 2012. Relative permeability calculations from two-phase flow simulations directly on digital images of porous rocks. Transp. Porous Media 94, 487–504.
Reynolds, C., Blunt, M., Krevor, S., 2014. Impact of reservoir conditions on CO_2-brine relative permeability in sandstones. Energy Procedia 63, 5577–5585.
Richardson, J.G., Kerver, J.K., Hafford, J.A., Osoba, J.S., 1952. Laboratory determination of relative permeability. Pet. Trans. AIME 195, 187–312.
Sandberg, C.R., Gournay, L.S., Sippel, R.F., 1958. The effect of fluid-flow rate and viscosity on laboratory determination of oil-water relative permeability. Pet. Trans. AIME 213, 36–43.
Shafer, J.L., Braun, E.M., Wood, A.C., Wooten, J.M., 1990. "Obtaining relative permeability data using a combination of steady-state and unsteady-state core floods" SCA 9009 Annual Symposium of the Society of Core Analysts Houston, Texas, pp. 1–16.
Sheng, Q., Thompson, K.E., Fredrich, J.T., Salino, P.A., 2011. Numerical Prediction of Relative Permeability from MicroCT Images: Comparison of Steady-State versus Displacement Methods. SPE 147431, 1–16.
Talash, A.W., 1976. "Experimental and Calculated Relative Permeability Data for Systems Containing Tension Additives" AIME SPE5810, 177–188.
Tallakstad, K.T., Knudsen, H.A., Ramstad, T., Løvoll, G., Maløy, K.J., Toussaint, R., Flekkøy, E.G., 2009. Steady-State Two-Phase Flow in Porous Media: Statistics and Transport Properties. Phys. Rev. Lett. 102 (074502), 1–4.
Tsakiroglou, C.D., Aggelopoulos, C.A., Terzi, K., Avraam, D.G., Valavanides, M.S., 2015. Steady-state two-phase relative permeability functions of porous media: A revisit. Int. J. Multiph. Flow. 73, 34–42. http://dx.doi.org/10.1016/j.ijmultiphaseflow.2015.03.001.
Tsakiroglou, C.D., Avraam, D.G., Payatakes, A.C., 2007. Transient and steady-state relative permeabilities from two-phase flow experiments in planar pore networks. Adv. Water Resour. 30, 1981–1992. http://dx.doi.org/10.1016/j.advwatres.2007.04.002.
Valavanides, M.S., 1998. Macroscopic theory of two-phase flow in porous media based on integration of pore scale phenomena. pH.D. dissertation, University of Patras, Greece. (⟨http://phdtheses.ekt.gr/eadd/handle/10442/11044?locale=en⟩ & http://users.teiath.gr/marval/publ/Valavanides_PhD_1998.pdf) (accessed 6/5/2016).
Valavanides M.S., Payatakes A.C., 2003. Prediction of Optimum Operating Conditions for Steady-State Two-Phase Flow in Pore Network Systems Using the *DeProF* True-to-Mechanism Theoretical Model. SCA2003–18, 2003 International Symposium of the Society of Core Analysts, Pau, France, 21–25 Sept., ⟨http://users.teiath.gr/marval/publ/Valavanides_Payatakes_SCA2003_18_2003.pdf⟩ (accessed 24/8/2015).
Valavanides, M.S., 2012. Steady-State Two-Phase Flow in Porous Media: Review of Progress in the Development of the *DeProF* Theory Bridging Pore- to Statistical Thermodynamics- Scales. Oil Gas. Sci. Technol. 67, 787–804. http://dx.doi.org/10.2516/ogst/2012056.
Valavanides, M.S., 2013. Transformer for steady-state relative permeability data ImproDeProF Project, ⟨http://users.teiath.gr/marval/ArchIII/relpermtrans.xls⟩ (accessed).
Valavanides, M.S., 2014. Operational Efficiency Map and Flow Characterization for Steady-State Two-Phase Flows in Porous Media. Society of Core Analysts Symposium - SCA2014, Avignon, France, September 8–14 (⟨http://users.teiath.gr/marval/publ/Valavanides_SCA2014–047.pdf⟩) (accessed 15/4/2015).
Valavanides, M.S., Tsakiroglou, C.D., Ioannidis, M.A., Vizika, O., 2015a. Unconventional modeling of multi-phase flows in porous media. Minisymposium 1.03, 7th International Conference on Porous Media, Padova, Italy, May 18–21 (⟨http://www.interpore.org/padova⟩ accessed 15/4/2015).
Valavanides, M.S., Totaj, E., Tsokopoulos, M., 2015b. Retrospective Examination of Relative Permeability Data on Steady-State 2-pH Flow in Porous Media Transformation of Rel-Perm Data (k_{ro}, k_{rw}) into Operational Efficiency Data (f_{EU}). ImproDeProF /Archimedes III, project internal report, ⟨http://users.teiath.gr/marval/ArchIII/retrorelperm.pdf⟩ (accessed 24/8/2015).
Van de Merwe, W., Nicol, W., 2009. Trickle flow hydrodynamic multiplicity: Experimental observations and pore-scale capillary mechanism. Chem. Eng. Sci. 64, 1267–1284. http://dx.doi.org/10.1016/j.ces.2008.10.069.
Virnovsky, G.A., Guo, Y., Skjaeveland, S.M., Ingsoy, P., 1995. Steady-state relative permeability measurements and interpretation with account for capillary effects. SCA 9502 Annual Symposium of the Society of Core Analysts, 1–10.
Virnovsky, G.A., Vatne, K.O., Skjaeveland, S.M., Lohne, A., 1998. Implementation of multirate technique to measure relative permeabilities accounting for capillary effects. SPE 49321, New Orleans, Louisiana, 901–911.
Vizika, O., Avraam, D.G., Payatakes, A.C., 1994. On the role of viscosity ratio during low-capillary-number forced imbibition in porous media. J. Colloid Interface Sci. 165, 386–401.
Wang, F.H.L., 1988. Effect of wettability alteration on water/oil relative permeability dispersion and flowable saturation in porous media. SPERE 15019, 617–628.
Wyckoff, R.D., Botset, H.G., 1936. The Flow of GasLiquid Mixtures Through Unconsolidated Sands. Physics 7 (325), 325–345. http://dx.doi.org/10.1063/1.1745402.
Youssef, S., Rosenberg, E., Deschamps, H., Oughanem, R., Maire, E., Mokso, R., 2014. Oil ganglia dynamics in natural porous media during surfactant flooding captured by ultra-fast x-ray microtomography. SCA 2014–23, Symposium of the Society of Core Analysts, France, 11–18 Sept, 1–12.